HHS Public Access

Author manuscript

Nature. Author manuscript; available in PMC 2021 February 02.

Published in final edited form as:

Nature. 2020 July ; 583(7816): 415–420. doi:10.1038/s41586-020-2395-5.

A neurotransmitter produced by gut bacteria modulates host sensory behaviour

Michael P. O'Donnell[1,3], **Bennett W. Fox**[2], **Pin-Hao Chao**[1], **Frank C. Schroeder**[2], **Piali Sengupta**[1,3]

[1]Department of Biology, Brandeis University, Waltham, MA 02454

[2]Boyce Thompson Institute and Department of Chemistry and Chemical Biology, Cornell University, Ithaca, NY 14853

Abstract

Animals coexist in commensal, pathogenic or mutualistic relationships with complex communities of diverse organisms including microbes[1]. Some bacteria produce bioactive neurotransmitters which have been proposed to modulate host nervous system activity and behaviors[2,3]. However, the mechanistic basis of this microbiota-brain signaling and its physiological relevance is largely unknown. Here we show that in *C. elegans,* the neuromodulator tyramine produced by gut-colonizing commensal *Providencia* bacteria bypasses the requirement for host tyramine biosynthesis to manipulate a host sensory decision. Bacterially-produced tyramine is likely converted to octopamine by the host tyramine β-hydroxylase enzyme. Octopamine in turn targets the OCTR-1 octopamine receptor on the ASH nociceptive neurons to modulate an aversive olfactory response. We identify genes required for tyramine biosynthesis in *Providencia,* and show that these genes are necessary for modulation of host behavior. We further find that *C. elegans* colonized by *Providencia* preferentially select these bacteria in food choice assays, and that this selection bias requires bacterially produced tyramine and host octopamine signaling. Our results demonstrate that a neurotransmitter produced by gut microbiota mimics the functions of the cognate host molecule to override host control of a sensory decision, thereby promoting fitness of both host and microbe.

[3]Correspondence and requests for materials should be addressed to M.P.O. mikeod38@gmail.com or P.S. sengupta@brandeis.edu.

Author Contributions

M.P.O, B.W.F, F.C.S and P.S. designed experiments, interpreted results and wrote the paper with input from all authors. M.P.O and P.H.C conducted long-range chemotaxis behavioral experiments and analyzed results. B.W.F conducted HPLC-MS experiments and analyzed results. M.P.O. conducted and analyzed results from all additional experiments.

Competing Interest Statement

The authors declare no competing interests.

Supplementary Information is available for this paper.

Data Availability Statement

All statistical analysis code and data necessary to reproduce these analyses are available as uploaded Source Data and/or at https://github.com/SenguptaLab/ProvidenciaChemo.git. Raw data from HPLC-MS experiments are available upon request due to large file sizes.

The pathways mediating chemical communication between gut-colonizing bacteria and host nervous systems are largely undescribed[3]. Recently, the nematode *C. elegans* has emerged as a powerful experimental system in which to study host-microbe chemical communication[4]. Diverse populations of pathogenic and non-pathogenic bacteria both colonize the *C. elegans* intestine and serve as its primary food source in the wild[5]. Exposure to pathogenic bacteria alters *C. elegans* olfactory behaviors[6], but whether commensal gut bacteria also modulate host behaviors is unknown.

Gut bacteria alter olfactory behavior

To identify novel modes of microbial influence on host behaviors, we screened non-pathogenic bacterial strains typically associated with wild nematodes[7] for their ability to influence *C. elegans* olfactory responses. In long-range population chemotaxis assays[8], adult hermaphrodites co-cultivated on these bacterial strains exhibited robust attraction to a panel of attractive volatile odorants similar to the behaviors of animals grown on the standard *E. coli* food source OP50 (Extended Data Fig. 1a). However, co-cultivation with the *Providencia alcalifaciens* strain (JUb39)[7,9] resulted in decreased avoidance of the volatile repellent 1-octanol, but not of the repellents 2-nonanone and 8M glycerol, as compared to OP50-grown animals (Fig. 1a, Extended Data Fig. 1b). This decreased avoidance is henceforth referred to as octanol modulation. Animals grown on a distantly-related *Providencia rettgeri* strain isolated from nematodes in compost (PYb007, Extended Data Fig. 1c) exhibited similar octanol modulation (Fig. 1b). These observations indicate that upon co-culture, multiple *Providencia* strains modulate octanol aversion in *C. elegans.*

Under specific conditions, food deprivation reduces octanol avoidance[10]. JUb39 has been categorized as a 'beneficial' bacterium that supports robust *C. elegans* growth and does not induce stress responses[7], suggesting that JUb39-fed animals are unlikely to be nutrition-deprived. Consistently, growth on JUb39 did not alter expression of a *tph-1*p*::gfp* fusion gene, a reporter of feeding state[11,12] (Extended Data Fig. 1d). Moreover, growth of *C. elegans* on the poor bacterial food *Bacillus megaterium*[13] did not alter octanol avoidance (Fig. 1a). We infer that the observed octanol modulation by *Providencia* is unlikely to be solely due to changes in feeding state.

While OP50 is typically crushed by the pharyngeal grinder in young adult *C. elegans*[14], a subset of bacterial strains can bypass the grinder and survive in the worm intestine[7,15,16]. Feeding *C. elegans* with JUb39 pre-treated with the antibiotic gentamicin eliminated octanol modulation (Fig. 1c). In addition, neither exposure of OP50-grown animals to JUb39-derived odors, nor pre-incubation of OP50-grown animals with JUb39-conditioned media altered octanol responses (Extended Data Fig. 1e–f), suggesting that *C. elegans* must ingest live JUb39 to induce octanol modulation.

To test whether colonization of the worm gut drives octanol modulation, we transformed OP50 and JUb39 with a plasmid encoding a constitutively-expressed mCherry fluorescent reporter. While the guts of OP50-fed adult worms displayed only diffuse intestinal fluorescence consistent with these bacteria being lysed, the guts of JUb39-fed worms contained typically large numbers of intact rod-shaped cells expressing mCherry (Fig. 1d).

Large numbers of bacterial colonies could be isolated after crushing JUb39-fed, but not OP50-fed worms following surface bleaching (Fig. 1e), indicating that JUb39 is likely alive in the nematode intestine. JUb39 cells tended to be enriched in the posterior intestine (Fig. 1d), unlike the reported localization pattern of severely pathogenic bacteria[17]. Moreover, nematodes colonized by JUb39 did not exhibit phenotypes characteristic of pathogenic infection such as anal swelling[18] (Fig. 1d), and had a similar lifespan to OP50-fed worms (Extended Data Fig. 1g), further confirming that JUb39 is largely non-pathogenic to *C. elegans.* We performed additional chemotaxis assays with animals fed mCherry-labeled JUb39, and quantified intestinal bacterial cells in animals that had navigated either toward octanol or the control. We found that animals navigating toward octanol consistently contained more gut bacteria (Fig. 1f). We conclude that JUb39 colonizes the worm gut, and the extent of colonization is correlated with decision-making in response to octanol.

Providencia bacteria produce tyramine

We next investigated the mechanistic basis for *Providencia*-mediated octanol modulation. Octanol avoidance is subject to extensive modulation directly and indirectly via multiple biogenic amines including tyramine (TA) and octopamine (OA), as well as neuropeptides[10,19–23]. TA is produced from Tyrosine (L-Tyr) via the activity of a tyrosine decarboxylase (TDC; encoded by *tdc-1* in *C. elegans*); TA is subsequently converted to OA via tyramine beta hydroxylase (encoded by *tbh-1*)[24] (Fig. 2a). Consequently, all *tbh-1* mutant phenotypes resulting from lack of OA are expected to be shared by *tdc-1* mutants[24]. Unexpectedly, we found that while *tdc-1* mutants grown on JUb39 continued to exhibit octanol modulation, the modulation exhibited by *tbh-1* mutants was reduced (Fig. 2b). Mutations in the *cat-2* tyrosine hydroxylase[25] and *tph-1* tryptophan hydroxylase[26] enzymes required for the production of dopamine and serotonin in *C. elegans*, respectively, did not affect octanol modulation (Fig. 2b). These results raise the possibility that *C. elegans*-produced OA, but not TA, is partly necessary for JUb39-mediated octanol modulation.

To account for these observations, we hypothesized that JUb39 may produce TA that functionally compensates for the host *tdc-1* mutation. *tdc-1* mutants grown on OP50 have been reported to display more rapid aversive responses to dilute (30%) octanol, which is suppressed by exogenous TA[19]. Monoaminergic modulation of octanol responses has typically been assessed via short-range acute avoidance assays [the "smell-on-a-stick" (SOS) assay][10,27] performed on individual animals (Fig. 2c). In this assay, the strength of avoidance is inversely correlated with reversal latency when the animal encounters the repellent as it is moving forward. To more easily permit comparisons with data from previously published work, and to gain insight into the behavioral subprograms altered by JUb39, we performed all subsequent octanol behavioral experiments using SOS assays. As expected, *tdc-1* mutants grown on OP50 responded more rapidly to 30% octanol than wild-type animals in SOS assays (Fig. 2d). This enhanced aversion was suppressed upon growth on JUb39 (Fig. 2d). These results are consistent with the notion that bacterially-produced TA functionally complements for the loss of host-derived TA in driving a sensory behavioral decision.

We performed metabolomic analyses to test whether growth on JUb39 compensates for the loss of TA and its metabolites in *tdc-1* worms. Using HPLC-HRMS[28] we found that *tdc-1* worms grown on OP50 were deficient in *N*-succinyl TA as reported previously[24], as well as additional metabolites that appear to be TA-derived based on MS2 analysis (Fig. 2e, Extended Data Figs. 2–5). Metabolism of serotonin was largely unperturbed (Extended Data Fig. 6). Production of these TA-derived metabolites was restored when *tdc-1* mutant worms were grown on JUb39 (Fig. 2e, Extended Data Figs. 3, 4d, 5d). Metabolomic analysis of *tdc-1* worms grown on JUb39 supplemented with stable isotope labeled D_2-L-tyrosine confirmed *de novo* biosynthesis of the TA moiety (Fig. 2f). We did not detect either free TA or TA conjugates in the absence of *C. elegans*. We conclude that JUb39 in association with *C. elegans* produces TA which can compensate for the lack of endogenous TA production in *tdc-1* mutant worms.

Although TA biosynthesis in bacteria has been demonstrated in some Gram-positive genera, production appears to be uncommon in Gram-negative bacteria which include *Providencia*[29,30]. TA production in Gram-positive strains is induced upon supplementation with L-Tyr[31]. We found that growth on L-Tyr-supplemented media enhanced octanol modulation by JUb39 in SOS assays (Extended Data Fig. 7a). Mutations in *tbh-1* fully suppressed octanol modulation in SOS assays, whereas *tdc-1* mutants continued to exhibit robust octanol modulation (Fig. 2g), consistent with our observations in long-range chemotaxis assays (Fig. 2b). Moreover, octanol avoidance behaviors of *tdc-1; tbh-1* double mutants were similar to those of *tbh-1* mutants alone (Fig. 2g), indicating that the lack of host-derived OA, and not accumulation of TA due to loss of TBH-1[24,28] accounts for the reduced octanol modulation in *tbh-1* mutants. Expression of wild-type genomic *tbh-1* sequences rescued octanol modulation in *tbh-1* mutants (Fig. 2g). Consistent with a role for neuronal OA release in octanol modulation, animals mutant for the neuron-specific *cat-1* vesicular monoamine transporter[32] were also deficient in octanol modulation (Extended Data Fig 7b).

Bacterial decarboxylases generate tyramine

Biogenic amines are typically generated from aromatic amino acids and L-glutamate by pyridoxyl phosphate (PLP)-dependent group II aromatic acid decarboxylase enzymes (AADCs) in both eukaryotes and bacteria[33]. In Gram-positive *Enterococcus* and *Lactobacillus (Lb)*, TA production is mediated by the TDC-encoding (*tyrDC*) AADC and tyrosine permease/transporter (*tyrP*) genes present in an operon; this operon is inducible by L-Tyr (Fig. 3a, Extended Fig. 8a–c, SI Table 1)[34,35]. Although genes related to *Enterococcus tyrDC* and *tyrP* were largely absent in *Gammaproteobacteria* (Extended Fig. 8c), we confirmed the presence of homologous operons containing *tyrDC* and *tyrP* in JUb39 and PYb007 in *de novo* genome assemblies via whole genome sequencing (Fig. 3a, SI Table 1). *tyrDC* homologs were also identified in the genomes of additional members of the *Morganellaceae* family, although the operon structure was conserved in only a subset of these genomes (Fig. 3a–b, SI Table 1).

Providencia TyrDC is highly homologous to the *Lb* enzyme, which has been well characterized with respect to substrate specificity[36]. Protein modeling using the crystal

structure of *Lb*-TyrDC[36] as a guide (see Methods) indicated that JUb39 TyrDC shares most known catalytic sites with *Lb*-TyrDC (Extended Data Fig. 8d). Interestingly, JUb39 TyrDC contains a substitution at A600 (S586 in *Lb*-TyrDC; Extended Data Fig. 8d), a variant demonstrated to enhance specific catalytic activity of *Lb*-TyrDC for tyrosine[36]. We infer that JUb39 TyrDC likely generates TA from tyrosine.

Morganella strains (*Morganellaceae* family) have been reported to produce TA under certain conditions[29], despite having no discernible *tyrDC* orthologs (Fig. 3b, Extended Data Fig. 8a–c, SI Table 1). Instead in *Morganella,* we identified an AADC-encoding gene (hereafter *adcA*) with ~29% and 27% sequence identity to *Enterococcus* TyrDC and human GAD67, respectively, in an operon upstream of a gene encoding a TYT-1 family putative tyrosine permease (Fig. 3a–b)[37]. An *adcA* homolog is also present in *Providencia* genomes, including in JUb39, but is not adjacent to a tyrosine transporter (Fig. 3a–b, Extended Data Fig. 8a–c, SI Table 1). We conclude that *Providencia* encodes at least two AADCs with the potential to generate TA, and the phylogenetic incongruence suggests that both *tyrDC* and *adcA* genes in the *Morganellaceae* family may have either been lost or acquired via horizontal gene transfer.

To test whether one or both JUb39 AADCs are necessary for octanol modulation, we engineered deletions in JUb39 *tyrDC* and *adcA (ΔtyrDC*::cmR and *ΔadcA*, respectively; Fig. 3a). Whereas cultivation on each of the bacterial single mutants weakly decreased octanol modulation, growth of wild-type *C. elegans* on the JUb39 *ΔtyrDC*::cmR *ΔadcA* double knockout bacteria abolished octanol modulation (Fig. 3c). We confirmed that JUb39 *ΔtyrDC*::cmR *ΔadcA* colonizes the *C. elegans* gut (Extended Data Fig. 9a). In contrast to wild-type JUb39, comparative metabolomics analyses showed that *tdc-1* worms grown on the JUb39 *ΔtyrDC*::cmR *ΔadcA* double mutant bacterial strain did not produce *N*-succinyl TA or other TA-derived metabolites (Fig. 3d–e, Extended Data Figs. 3, 4d, 5d). Octanol modulation was restored in wild-type *C. elegans* grown on JUb39 *ΔtyrDC*::cmR *ΔadcA* strains upon supplementation with TA (Fig. 3f). Moreover, while exogenous TA did not further increase octanol avoidance in wild-type JUb39-grown animals, TA supplementation was sufficient to induce octanol modulation in OP50-grown animals (Fig. 3f). Together, these results indicate that TA produced by multiple AADC enzymes in *Providencia* is both necessary and sufficient to modulate octanol avoidance by wild-type *C. elegans*.

TA regulates behaviors such as egg-laying in *C. elegans*[24,38]. We asked whether TA produced by AADC enzymes in *Providencia* is sufficient to suppress egg-laying defects of *tdc-1* mutants, in addition to modulating octanol avoidance indirectly via OA. We found that while as reported, *tdc-1* mutants grown on OP50 contained on average younger eggs *in utero* than wild-type animals[24], growth on wild-type JUb39, but not on JUb39 *ΔtyrDC*::cmR *ΔadcA,* suppressed this egg-laying defect of *tdc-1* mutants (Extended Data Fig. 10). These results indicate that TA produced by JUb39 in worms complements multiple *tdc-1* dependent phenotypes.

Bacterial tyramine targets sensory neurons

We next sought to identify the molecular targets of *Providencia*-mediated octanol modulation in the host. The bilateral ASH nociceptive neurons in the head amphid organs of *C. elegans* have been implicated in sensing octanol[10,20,27]. These neurons express multiple TA and OA receptors, a subset of which is required for octanol modulation by these monoamines[19,39]. Among ASH-expressed OA receptors, mutations in *octr-1*, but not *ser-3,* abolished JUb39-mediated octanol modulation, without altering the extent of gut colonization (Fig. 4a, Extended Data Fig. 9). We also observed an effect on octanol modulation in *tyra-2* TA receptor mutants, primarily due to decreased octanol avoidance upon growth on OP50 (4.3 ± 0.25 sec for *tyra-2* vs. 2.9 ± 0.13 sec for WT) (Extended Data Fig. 9b). Expression of *octr-1* cDNA in the ASH but not ASI sensory neurons fully restored octanol modulation (Fig. 4a). *octr-1* mutants also lacked octanol modulation when grown on JUb39 *ΔtyrDC*::cmR *ΔadcA* supplemented with TA (Fig. 4b). OCTR-1 has been shown to inhibit innate immune responses to pathogens in *C. elegans* via suppression of an unfolded protein response pathway[40]. However, the observations that JUb39 does not induce expression of virulence, stress or unfolded protein response genes[7], and only minimally affects *C. elegans* longevity (Extended Data Fig. 1g), together with the well-established role of ASH in OA-modulated octanol avoidance[10,19–21], suggest that the observed octanol behavioral phenotypes are unlikely to arise from changes in innate immune responses in JUb39-grown animals.

Bacterial tyramine biases feeding choices

We next investigated the biological relevance of the JUb39-directed decrease in aversive olfactory responses by *C. elegans*. While many Gram-negative enteric bacteria produce long-chain alcohols including octanol[41], whether *Providencia* produces this chemical is unknown. However, JUb39 and other *Providencia* strains produce the branched alcohol isoamyl alcohol (IAA), which is aversive to *C. elegans* when concentrated[42,43]. Similar to octanol, avoidance of high IAA concentrations is also mediated by the ASH sensory neurons[43]. We hypothesized that reduced avoidance of JUb39-produced aversive alcohols or other odorants may preferentially bias JUb39-grown *C. elegans* to select these bacteria in food choice assays (Fig. 4c). Indeed, animals grown on JUb39 preferred JUb39 as compared to OP50-grown worms, which showed only a slight preference for JUb39 in a short-range food choice assay (Fig. 4d). The bias towards JUb39 was largely eliminated in animals grown on JUb39 *ΔtyrDC*::cmR *ΔadcA* (Fig. 4d), as well as in *octr-1* and *tbh-1* mutants (Fig. 4e) suggesting that both bacterial TA production and host OA signaling are necessary for this food preference. Together, these results imply that TA produced by JUb39 in the worm intestine acts via host OA and the OCTR-1 OA receptor to reduce ASH-mediated avoidance of JUb39-produced aversive cues such as concentrated alcohols and allow preferential selection of these bacteria (Fig. 4f).

Discussion

Our observations support a model in which the neurotransmitter TA produced by intestinal *Providencia* bacteria can subvert host-dependent TA production to modulate multiple

monoaminergic pathways and alter behavior and physiology in *C. elegans.* Bacterially-produced TA is converted to OA by *C. elegans* TBH-1; OA subsequently acts on the ASH neurons via the OCTR-1 OA receptor to decrease aversion of enteric bacterially-produced volatiles such as octanol, and alter food choices (Fig. 4f). We speculate that the preference for *Providencia* upon colonization of *C. elegans* by these bacteria promotes increased consumption leading to stable association[5,44] and bacterial dispersal. As *Providencia* is a rich food source for *C. elegans*[7], this association may be mutually beneficial. Other metabolites from commensal bacteria have been shown to have a beneficial effect on feeding decisions as well as maintenance and dispersal of these bacteria in *Drosophila*[45–47], and intestinal bacteria can modulate satiety responses in mammals via largely uncharacterized mechanisms[48,49]. Our results describe a pathway by which neurotransmitters produced by natural commensal bacteria direct host sensory behavioral decisions by supplementing or compensating for the activity of key host biosynthetic enzymes, thereby altering fitness of both host and microbe.

METHODS

Strains

C. elegans: All *C. elegans* strains were maintained on nematode growth medium (NGM) at 20°C, and hermaphrodites were used for all experiments. *srv-11*p*::octr-1* (pMOD110) and *srg-47*p*::octr-1* (pMOD111) plasmids were injected at 10 ng/μL, *tbh-1*p*::tbh-1a::SL2::mcherry* (pMOD115) was injected at 20ng/μL together with the *unc-122*p*::mcherry* coinjection marker at 30 ng/μL to generate transgenic strains. At least two independent lines were examined for all rescue experiments. Strain genotypes are listed in SI Table 2.

Bacteria: For all experiments, bacterial strains were streaked from glycerol stocks prior to use and grown to saturation in LB media at 37°C. For conditioned media, bacteria were grown to saturation in NGM media overnight at 37°C, then cleared by centrifugation at 14,000g for 3 mins. Prior to use, conditioned media or NGM was supplemented with 5x concentrated OP50 from a saturated LB culture to prevent starvation. To expose animals to bacterial odors, worms were grown on seeded NGM plates whose lids were replaced with NGM plates containing the test bacteria; these were sealed with parafilm. For L-Tyr and TA supplementation experiments, 0.5% (~28mM) L-Tyr (Sigma T3754) or 4mM or 10mM TA (Sigma T2879) were added to the NGM media and agar prior to pouring plates. To generate antibiotic-killed bacteria, saturated cultures of OP50 or JUb39 were concentrated 5x by centrifugation followed by resuspension in LB media containing 200 μg/mL gentamicin (Sigma G1397) for 4 hours at 37° C. Four 100 μL spots of this treated bacteria suspensions were added to 10 cm NGM plates and allowed to dry before adding L4 stage worms.

Plasmids were transformed into JUb39 and OP50 via electroporation. Deletions in JUb39 were induced using homologous recombination with the temperature-sensitive pSC101 replicon at 42°C, and sacB-sucrose counter-selection at 30°C, in the absence of NaCl as described[50], with the exception that bacteria were incubated for 1 hr at room temperature in the presence of 10mM arabinose for lambda Red induction prior to selection at 42°C.

Deletions were confirmed by sucrose resistance and kanamycin sensitivity, followed by PCR and sequencing of deleted intervals.

Molecular biology

The *octr-1* cDNA was a gift from Dr. Richard Komuniecki. The cDNA was amplified by PCR and cloned using Gibson homology cloning. The 1940bp *srv-11* promoter and 978bp *srg-47* promoter sequences were cloned from genomic DNA. *tbh-1a* cDNA was amplified from a mixed-stage cDNA pool by PCR. The 1357bp *tbh-1* promoter plasmid was a gift from Mark Alkema. Vector maps are available on Github (https://github.com/SenguptaLab/ProvidenciaChemo.git). For introduction of deletions via homologous recombination in JUb39, pKD46-derivative plasmids containing a lambda Red cassette and deletion homology arms for JUb39 *tyrDC* and *adcA* were constructed (denoted pMOD102 and pMOD107, respectively). Briefly, the *cas9* coding region and sgRNA regions of pDK46-derivative pCAS[51] were deleted and replaced with the *sacB* sequence from pCM433[52] via PCR and Gibson homology cloning. For pMOD102, 5' and 3' homology arms were approximately 400bp each flanking a 1233bp deletion of the *tyrDC* coding sequence which was replaced with a chloramphenicol resistance cassette. For pMOD107, 5' and 3' homology arms were 701 and 422bp, respectively, flanking a 1398bp deletion of the *adcA* CDS. For expression of mCherry in OP50 and JUb39, a pUCP20T-mCherry plasmid[53] was modified to replace *bla*(ampR) with *aph*(kanR).

Microscopy

All fluorescence and DIC microscopy was performed using animals anesthetized with 100mM levamisole (Sigma Aldrich). Animals were imaged on 2% agarose pads using an upright Zeiss Axio Imager with a 63X oil immersion objective.

Quantification of intestinal bacterial cell numbers: All rod-shaped punctae in the intestines of young adult worms of approximately 1-2μm were included in the quantification. Each animal was recorded in one of three categories containing 0, <10, or >10 cells per animal. Exact numbers in animals with > 10 cells were not recorded, but rarely exceeded approximately 100 cells.

Fluorescence intensity measurements: All images were collected in *z*-stacks of 0.5 μm through the heads of young adult worms. Quantification was performed using ImageJ (NIH). Fluorescence was quantified by identifying the focal plane in which the cell soma was visible, followed by manually drawing an ROI around the soma. Mean pixel intensity was recorded for each neuron pair per animal and the average of fluorescence in each animal is shown.

Quantification of intestinal colony forming units (cfu)

To estimate intestinal cell number, surface sterilization was performed as reported[54] with modifications. N2 young adult worms cultured for a single generation on OP50 or JUb39 were washed off a culture plate with M9 buffer, allowed to settle for 1–2 minutes followed by aspiration of supernatant. Animals were rinsed 4 more times with 1mL M9 buffer, followed by one rinse with M9 + 25mM levamisole (Sigma Aldrich) to block pharyngeal

pumping. Animals were then incubated with 1% bleach in M9 + 25mM levamisole for 5 min, followed by 5 more rinses with M9 buffer. 100µl of the final supernatant was plated on LB media as a wash control. Animals were then placed on an NGM plate, after which 10 young adult worms per condition were picked into separate tubes containing 100µL M9 buffer and were crushed using a pestle (UAS Scientific 1415–5390). The resulting samples were serially diluted and plated on LB media. CFU per 10 worms were normalized by subtracting the number of colonies observed in plates from the wash control.

C. elegans assays

Long-range chemotaxis: Long-range chemotaxis assays were performed essentially as described[8,55]. Worms were cultured for 1 generation with the relevant bacteria prior to the assay. Assays were performed using 10cm square NGM plates. The number of worms in two horizontal rows adjacent to the odor and ethanol spots were quantified.

SOS assays: Smell-on-a-stick (SOS) assays in response to 1-octanol or 2-nonanone were performed as described[10,27]. NGM plates were pre-dried for 1 hour prior to assays. Age-matched young adult animals were picked from food to a clean transfer plate and allowed to briefly crawl away from food for approximately 1 min. Animals were then transferred to another clean NGM plate for 15 mins prior to assaying responses to 100% octanol (Sigma O4500) and 100% 2-nonanone (Sigma 108731), or 20 mins for 30% octanol assays. 30% octanol was prepared immediately before the assay by dilution in 200-proof ethanol (Acros Organics 61509–0010).

Short-range bacterial choice assay: Animals were raised and prepared identically to those used in long-range chemotaxis assays, with the exception that the final wash with water was omitted. NGM plates containing two 15µL spots separated by 2 cm of overnight-grown bacterial food concentrated to OD600 = 10 were allowed to dry, then incubated with a closed lid for 5 hrs at room temperature. Approximately 30 animals were placed between the two spots, and excess liquid was removed. Animals were allowed to navigate for 15 mins following which 2µL of sodium azide was applied to each spot to anesthetize worms. Minimal lawn-leaving behavior was observed during this short time period. Adult animals on the control spot and test spot were counted.

Osmotic avoidance assay: Animals off the bacterial food on the cultivation plate were picked using a 10% methyl cellulose polymer solution and placed in the center of an NGM plate with a ring of 8M glycerol containing bromophenol blue (Sigma B0126). The number of worms inside and outside of the ring were counted after 10 mins.

Quantification of eggs in utero: N2 or *tdc-1* animals were grown from egg to the L4 stage on NGM plates containing either OP50, JUb39 or JUb39 *ΔtyrDC*::cmR *ΔadcA.* Age-matched L4 larvae were transferred to new plates 18h prior to the assay. The number of eggs younger or older than the 4-cell stage were recorded over 3 independent days of assays.

Lifespan assays: N2 animals were grown on 6cm NGM plates containing 100µL OP50, JUb39 or PA14. 20 L4 animals were placed on each plate at the beginning of the experiment.

4 replicate plates were analyzed for each condition per day over 3 independent days of experiments. Animals were transferred to new plates at least once every two days until they ceased to lay eggs. Animals were censored if they crawled off of the plate, exhibited *in utero* larval hatching ("bagging"), or if they were injured during transfers. Animals were scored as dead if they failed to respond to being prodded in the head.

Tyrosine supplement for metabolomics assay: *tdc-1* animals were grown on plates containing 0.5% L-Tyr (*w/v*) or at the same concentration containing a 1:1 mixture of L-Tyr and 3,3-D_2-L-Tyr, purchased from Cambridge Isotope Laboratories (DLM-2317-.5).

Bacteria genome sequencing

Sequencing was performed by the Broad Technology Labs at the Broad Institute. Resulting PacBio reads for JUb39 and PYb007 were assembled using Canu v1.8 (https://github.com/marbl/canu.git)[56]. Assemblies were trimmed, oriented and circularized using Circlator v1.5.5 (https://sanger-pathogens.github.io/circlator/)[57].

Phylogenetic analysis of group II pyridoxal-dependent decarboxylase genes

JUb39 TyrDC and AdcA were initially identified as the only significant hits via a tblastn search of the draft JUb39 genome assembly using *Enterococcus faecalis* TyrDC as a query sequence. An initial BLASTP screen of the nr sequence database restricted to bacteria was performed using the *P. alcalifaciens* JUb39 TyrDC and AdcA coding regions. Searches were performed hierarchically, limited initially to *Enterobacteriaceae*, followed by *Enterobacterales, Gammaproteobacteria, Proteobacteria* and finally all *Eubacteria.* With the exception of members of *Morganellaceae* (*Providencia, Proteus, Morganella, Xenorhabdus, Photorhabdus, Arsenophonus* and *Moellerella*), only two protein sequences per genus were retained for subsequent phylogenetic analysis. Representative group II decarboxylase enzymes with known substrate specificity from *Eukaryota* and *Archaea* as well as glutamate decarboxylase (*gadA/B*) and histidine decarboxylase sequences were also included.

Multiple sequence alignments were produced using the Phylomizer workflow (https://github.com/Gabaldonlab/phylomizer), which used the MUSCLE v3.8.31 (http://www.drive5.com/muscle)[58], MAFFT v7.407 (https://mafft.cbrc.jp/alignment/software)[59] and Kalign v2.04 (http://msa.sbc.su.se/cgi-bin/msa.cgi)[60] multiple sequence aligners; these were trimmed to produce a consensus alignment using trimAL v1.4rev15 (https://github.com/scapella/trimal)[61]. An initial phylogenetic tree was produced using PhyML v3.3.20180621 (http://www.atgc-montpellier.fr/phyml/)[62] using the NNI algorithm with an LG substitution model. This tree showed three major, well-supported clusters containing: (1) *Enterococcus* and *Providencia* TyrDCs - denoted "*Enterococcus*-type TDC", (2) Eukaryotic AADCs denoted "Eukaryotic-type AADC", and (3) *Morganella* AdcA and *Providencia* AdcA.

Based on this initial tree, a second tblastn search was used to determine the presence or absence of homologous genes among complete *Gammaproteobacteria* genomes. *Enterococcus faecalis* TyrDC and *C. elegans* TDC-1 were used as tblastn search query sequences. Hierarchical search was performed as described above, limited to an e-value

cutoff of 10^{-5}. A maximum of 2 highly similar sequences were retained per genus for phylogenetic analysis as listed in SI Table 1.

A final phylogenetic tree was constructed using the amino acid sequences derived from these tblastn queries. These were assembled into a consensus alignment using the Phylomizer workflow as described above. ProtTest (https://github.com/ddarriba/prottest3)[63] was used to identify the optimal model for likelihood estimation, using Aikake Information Criterion (AIC) values for selection. The model selected and subject to PhyML analysis was an LG model with discrete gamma distribution, an estimated proportion of invariant sites (+I), empirical frequencies of amino acids (+F), estimated gamma shape parameter (+G) for rate variation among sites with the default 4 substitution rate categories, and the subtree pruning and regrafting (SPR) algorithm. 100 bootstrap pseudoreplicates were analyzed. Representatives from the resulting phylogeny were used to categorize and compile the cladogram in Fig. 3b. Adjacent genomic sequences, up to 3 CDS 5' or 3', were examined for genes encoding amino-acid permeases or transporters in an apparent operon as defined by close proximity and same orientation with respect to each tblastn hit (SI Table 1).

Molecular modeling

The putative amino acid sequence for JUb39 TyrDC was used to model active site residues using the *Lb*-TyrDC crystal structure in complex with PLP (5hsj.1[36]) as a template guide using SWISS-MODEL (https://swissmodel.expasy.org)[64]. This resulted in a Qmean Z-score of 0.33, indicative of good agreement between structures. This process was also attempted with AdcA, and modeling was performed with the top 6 available structures based on sequence homology. The maximum QMean of AdcA was found with *Lb*-TyrDC, but with a value −5.71, indicative of low quality. Resulting models were visualized using Chimera v1.13.1 (https://www.cgl.ucsf.edu/chimera/)[65]. For Extended Data Fig. 8d, L-Tyrosine was manually docked according to the reported docking position[36] for illustrative purposes only.

Statistical analyses

All statistical analyses were performed in R (https://www.R-project.org/)[66] and RStudio (http://www.rstudio.com)[67]. Sample sizes were chosen according to conventional estimates of power for all assays. No randomization or blinding was performed. For modulation index and relative latency figures, data were normalized to the relevant control group mean value for each experimental day on the log scale via subtraction. Outliers in boxplots were defined as greater than 1.5 x interquartile range, but were included for analysis. All statistical analyses were performed on raw, non-normalized data. To avoid inflated *P*-values and to account for non-independence of observations, we employed mixed-effects regression analysis in lieu of simple ANOVA and t-tests. For behavioral assays, frequentist statistical comparisons were performed using a binomial generalized linear mixed-effects model (GLMM) with a logit link function for chemotaxis, food choice and egg-*in-utero* assays, while a linear mixed-effects model (LMM) on $\log_{10}$-transformed data was used to analyze SOS assays using the 'lme4' package v1.1–21[68]. In all cases, a random intercept term for assay plate was used to account for non-independence of animals on each assay plate and random intercept for date was used to account for day-to-day variability. In the presence of interactions, for example, the effects of bacterial strains across different odorants in Fig. 1a

and Extended Data Fig. 1a, a random slope term per date was also used when appropriate. Estimated *P*-values for pairwise comparison of fixed effects were determined using Kenward-Roger approximated degrees of freedom as implemented in the 'emmeans' v1.4.5[69] and 'pbkrtest' v0.4–86[70] packages. In nearly all cases, inclusion of random effects model terms resulted in conservative *P*-value estimates compared to a simple ANOVA. In the event of singular model fit, any random slope term, followed by random date effect terms were removed to allow convergence. For Wald statistics of model terms, packages 'lmerTest' v3.1-1[71] or 'car' v3.0-6[72] were used.

Additionally, for each dataset, a maximal Bayesian model was fit using the 'rstanarm' v2.19.3[73] package. Data presented are posterior credible intervals for fixed effect levels derived from posterior fitted values of the MCMC chains as implemented by the 'emmeans', 'coda' v0.19-3[74], 'bayesplot' v1.7.1[75] and 'tidybayes' v2.0.1[76] packages. Post-hoc corrections for multiple comparisons and type-I error were implemented using the 'emmeans' package. For comparison of intestinal bacterial cell numbers, an ordinal logistic regression was performed using the 'MASS' v7.3-51.4[77] package and 'polr' function. Categories of cell numbers were considered ordered factors of 'none', 'some' or 'many' cells. All statistical analysis code and raw data are available (https://github.com/SenguptaLab/ProvidenciaChemo.git).

For survival analysis data were fit to a Gompertz-Makeham function using 'nls' function in R using the following equation: S(t) = e^(−(G/γ)*(e^(γt)−1)). Bootstrap confidence intervals were derived from 1000 bootstrap samples with replacement, followed by nls fit. To calculate bootstrap median survival, using each nls fit and solving for t at S = 0.5 yielded the equation: t = (1/γ)*ln(1−(γ/G)*ln(0.5)).

Sample preparation for HPLC-MS

Approximately 10,000 mixed-staged worms in 1.5mL microfuge tubes were lyophilized for 18-24 hrs using a VirTis BenchTop 4K Freeze Dryer. After the addition of two stainless steel grinding balls and 1mL of 80% methanol, samples were sonicated for 5 min (2 sec on/off pulse cycle at 90 A) using a Qsonica Q700 Ultrasonic Processor with a water bath cup horn adaptor (Model 431C2). Following sonication, microfuge tubes were centrifuged at 10,000 RCF for 5 min in an Eppendorf 5417R centrifuge. 800μL of the resulting supernatant was transferred to a clean 4mL glass vial, and 800μL of fresh methanol added to the sample. The sample was sonicated and centrifuged as described, and the resulting supernatant was transferred to the same receiver vial and concentrated to dryness in an SC250EXP Speedvac Concentrator coupled to an RVT5105 Refrigerated Vapor Trap (Thermo Scientific). The resulting powder was suspended in 120μL of 100% methanol, followed by vigorous vortex and brief sonication. This solution was transferred to a clean microfuge tube and subjected to centrifugation at 20,000 RCF for 10 min in an Eppendorf 5417R centrifuge to remove precipitate. The resulting supernatant was transferred to an HPLC vial and analyzed by HPLC-MS.

HPLC-MS analyses

Reversed-phase chromatography was performed using a Vanquish LC system controlled by Chromeleon Software (ThermoFisher Scientific) and coupled to an Orbitrap Q-Exactive High Field mass spectrometer controlled by Xcalibur software (ThermoFisher Scientific). Methanolic extracts prepared as described above were separated on an Agilent Zorbax Eclipse XDB-C18 column (150 mm x 2.1 mm, particle size 1.8 μm) maintained at 40 °C with a flow rate of 0.5 mL/min. Solvent A: 0.1% formic acid in water; solvent B: 0.1% formic acid in acetonitrile. A/B gradient started at 5% B for 3 min after injection and increased linearly to 98% B at 20 min, followed by 5 min at 98% B, then back to 5% B over 0.1 min and finally at 5% B held for an additional 2.9 min to re-equilibrate the column. Mass spectrometer parameters: spray voltage, −2.9 kV/+3.5 kV; capillary temperature 380 °C; probe heater temperature 400 °C; sheath, auxiliary, and sweep gas, 60, 20, and 2 AU, respectively; S-Lens RF level, 50, resolution 240,000 at *m/z* 200; AGC target, 3E6. Each sample was analyzed in negative (ESI-) and positive (ESI+) electrospray ionization modes with *m/z* range 150–800. Parameters for MS/MS (dd-MS2): MS1 resolution, 60,000; AGC Target, 1E6. MS2 resolution, 30,000; AGC Target, 2E5; maximum injection time, 50 msec; isolation window, 1.0 *m/z*; stepped normalized collision energy (NCE), 10, 30; dynamic exclusion, 5 seconds; top 10 masses selected for MS/MS per scan. LC-MS data were analyzed using Metaboseek software (see below) and quantification performed via integration in Excalibur Quan Browser (ThermoFisher Scientific).

Metabolic network analysis

MS2 networking was performed using Metaboseek MS analysis software (doi: 10.5281/zenodo.3360087)[78]. Documentation and source code are available in the Metaboseek R package on GitHub: https://mjhelf.github.com/Metaboseek. For additional information, installation instructions and a user guide, please visit https://metaboseek.com. The xcms package[79] within Metaboseek was used with "Metaboseek_default" settings, suitable for HRMS instruments, followed by MS2 matching using the following parameters: ppm window, 3; RT window, 5 seconds; 'unique assignments' on. From roughly 200,000 features detected in ESI+ HPLC-MS, approximately 10,000 features were matched to MS2 spectra, which was further culled to 4,563 features using the 'Peak Shapes' functionality to calculate peak quality scores, applying a threshold of 0.97. Networking was performed using the Compare MS2 function in Metaboseek with the following parameters: *m/z* tolerance, 0.002; ppm tolerance, 3; min. number of peaks in common, 4; noise level, 2%; with 'parent masses' turned on and 'ignore small fragments' (*m/z* < 100) turned on. The network was modified by removing edges below similarity score (cosine) = 0.7, and further simplified by restricting the maximum number of edges per node to the top 5 ranked by similarity score.

Extended Data

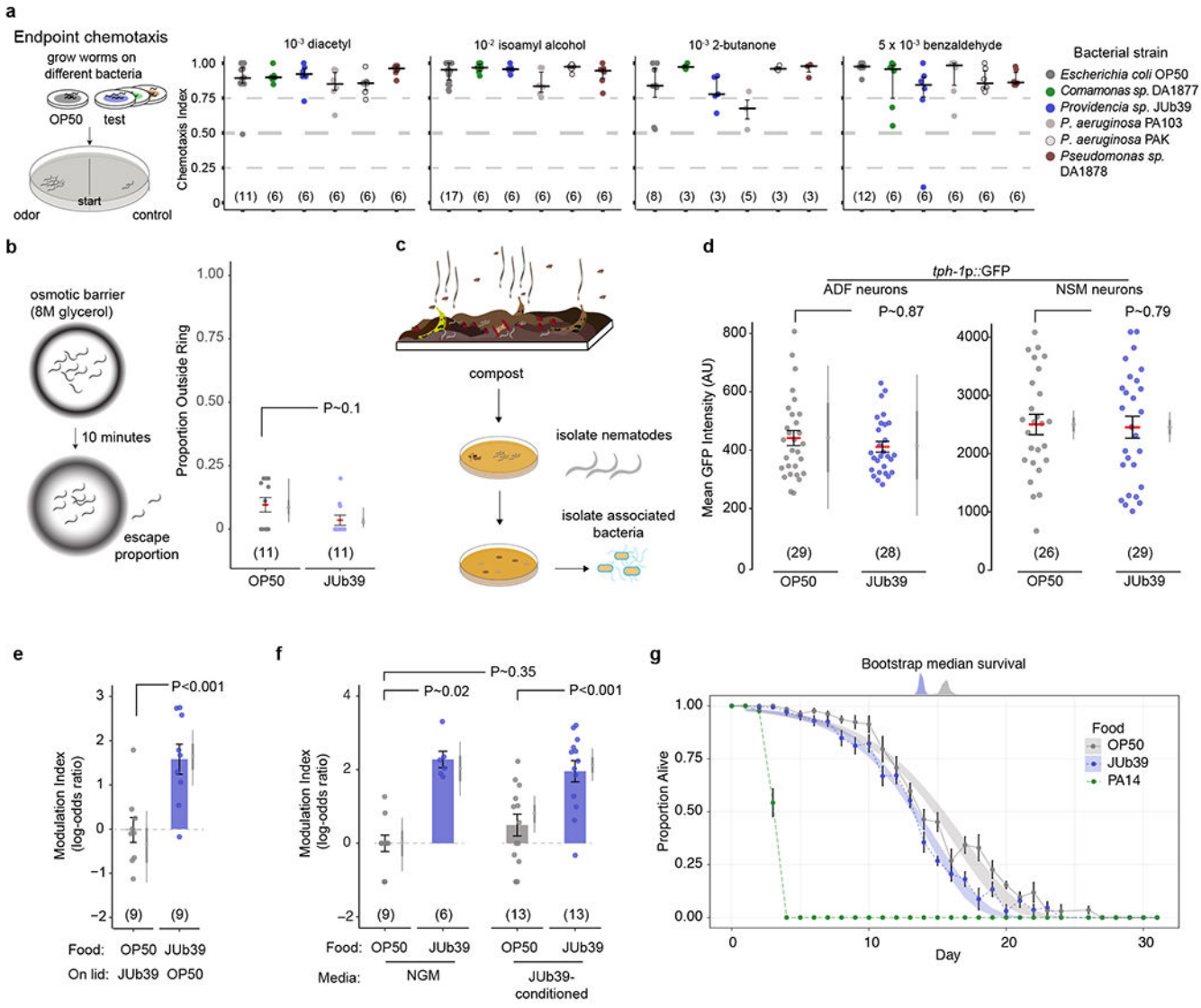

Extended Data Fig. 1. Octanol modulation by *Providencia* requires ingestion of bacteria and is not mediated by nutritive cues.

a, Cartoon and data from long-range chemotaxis assays of *C. elegans* grown on the indicated bacterial strains to the indicated attractive odors. Chemotaxis index (CI) = (animals at odorant – animals at control)/total animals. Dots, CI from single assays of approximately 100 animals. Horizontal line, median; errors, 1st and 3rd quartiles. Numbers in parentheses, number of assays performed over at least 3 days. **b,** Cartoon and data from osmotic ring avoidance assay. Dots, single assays of 10 animals. Numbers in parentheses, number of assays over at least 3 independent days. Y-axis is proportion of animals leaving an osmotic ring barrier of 8M glycerol after 10 minutes. *P*-value represents difference of means relative to JUb39-grown animals from a GLMM. Errors are SEM. Gray thin and thick vertical bars, Bayesian 95% and 66% credible intervals, respectively. **c,** Isolation of nematode-associated bacteria. Nematodes were isolated from residential compost in Massachusetts. Worms were

allowed to crawl onto NGM plates from which they were picked to clean plates. Resulting bacterial colonies were isolated, grown on LB media and characterized via 16S rRNA sequencing. **d,** Expression of a *tph-1*p*::gfp* fluorescent reporter in indicated head neurons of young adult animals grown on either OP50 or JUb39. Dots, mean fluorescence of the soma of single neurons. Horizontal bar is mean; errors are SEM. Gray thin and thick vertical bars, Bayesian 95% and 66% credible intervals, respectively. *P*-values are from two-way ANOVA. **e-f,** Modulation index of worms grown on the indicated bacterial strains to 100% octanol, under the shown conditions. Animals were exposed to the indicated bacteria on the plate lid (e) for one generation, or to NGM control or bacteria-conditioned NGM **(f)** for 2 hours prior to the assay. Numbers in parentheses, independent experiments over 2 days with approximately 100 animals each. Values are shown on a log-odds (logit) scale and are normalized to the values of wild-type animals grown on OP50 for each day, indicated with a gray dashed line. Positive numbers indicate reduced avoidance of octanol. Errors are SEM. Gray thin and thick vertical bars, Bayesian 95% and 66% credible intervals, respectively. *P*-values between the indicated conditions are post-hoc comparisons from a GLMM, with Tukey-type multivariate-t adjustment for **(f)**. **g,** Survival analysis of worms grown on the indicated strains. Dots, average proportion of surviving worms from 12 plates of 20 worms each on the indicated days. Error bars are SEM. Shaded blue and gray curves indicate 95% confidence intervals derived from 1000 bootstrap Gompertz function non-linear least squares (nls) fits of the indicated data. Top blue and gray distributions show bootstrapped median survival of the indicated strains.

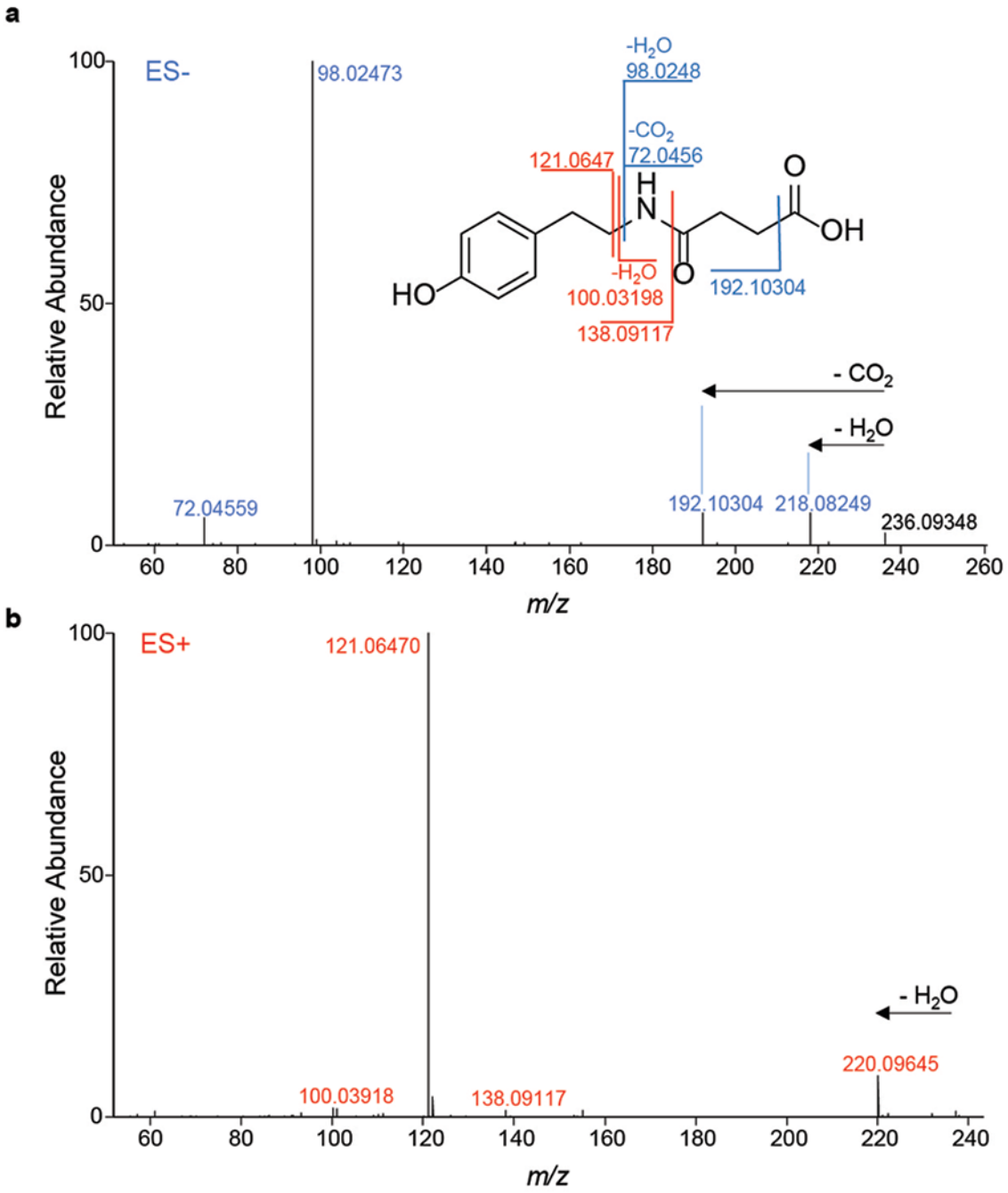

Extended Data Fig. 2. Detection of *N*-succinyl TA.

Major fragmentation reactions and resulting fragment ions are indicated in mass spectra of *N*-succinyl TA obtained in ESI− **(a)** and ESI+ **(b)** HPLC-MS2. Representative data are shown from at least three biologically independent experiments.

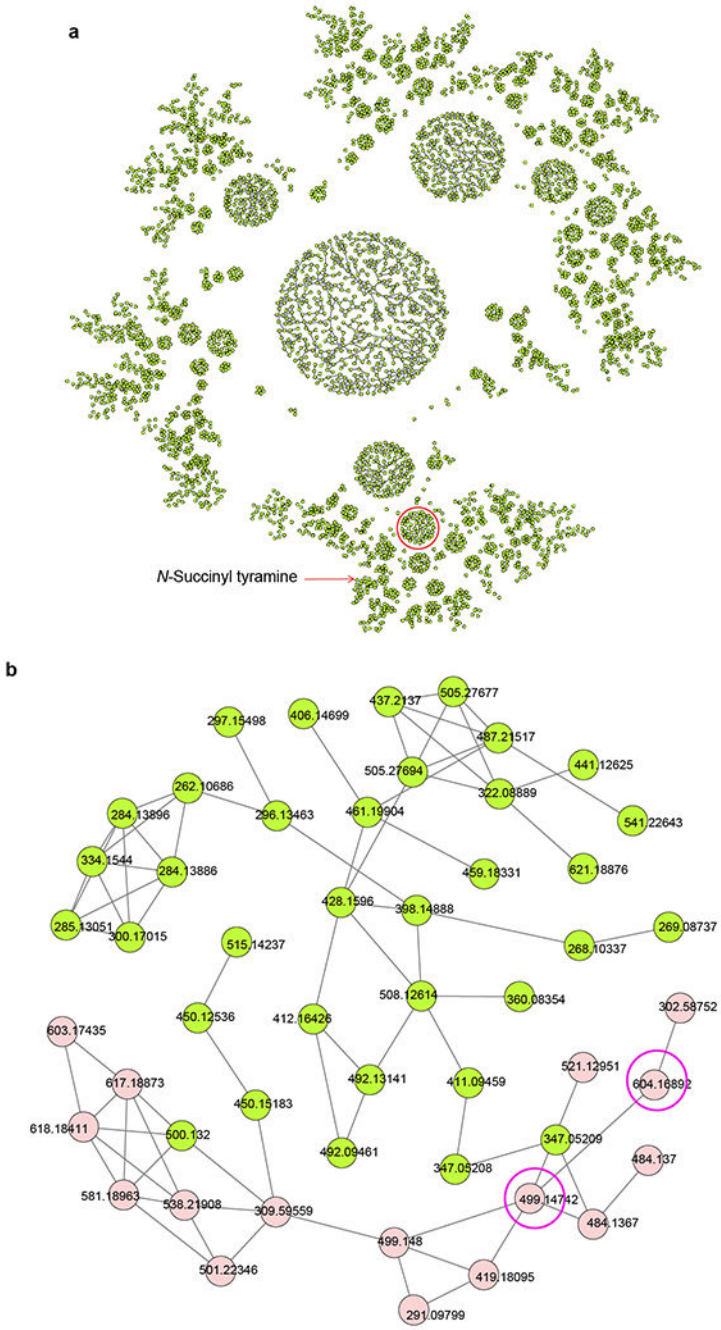

Extended Data Fig. 3. Complementation of TA-containing metabolites in *tdc-1* mutants via *Providencia* TDC-encoding genes.

a, Overview of MS2 network obtained in positive ion mode. Each node represents a unique feature, and edges between nodes indicate similarity between MS2 spectra. Red circle highlights the sub-network containing the majority (16 out of 24 features, representing 10 out of 15 differential compounds) of differential TA-containing metabolites. This sub-network contains glycosylated TA-derivatives, *N*-succinyl-TA is represented by a node in a different sub-network (red arrow). **b,** Magnified view of sub-network highlighted in **(a)**. The

TA-containing features restored upon growth of *tdc-1* worms on wild-type JUb39, and abolished when grown on JUb39 *ΔtyrDC*::cmR *ΔadcA*, are highlighted in light red. MS2 spectra for two example compounds at *m/z* 499.1474 and *m/z* 604.1689 (circled in magenta) are shown in Extended Data Figs. 4 and 5.

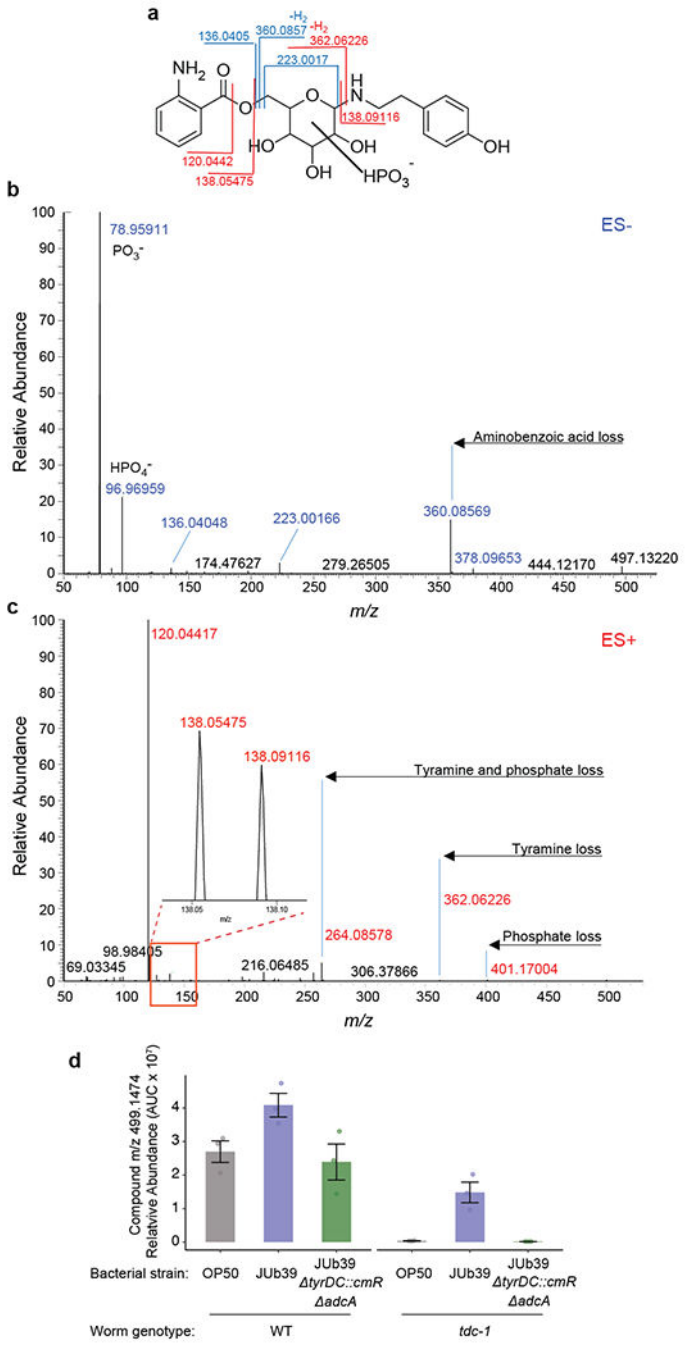

Extended Data Fig. 4. MS2 analysis and quantitation of TA-containing metabolite *m/z* 499.1474.

a, Major fragmentation reactions of *m/z* 499.1474 and resulting fragment ions. The shown putative structure is based on fragmentation and stable isotope incorporation.

Stereochemistry and exact substitution pattern are unknown. *b-c,* MS2 spectra obtained in **(b)** ESI- and **(c)** ESI+ mode. Representative data are shown from at least three biologically independent experiments. **d,** Quantification of *m/z* 499.1474 in wild-type and *tdc-1* worms fed the indicated bacterial strains as determined by positive-ion ESI+ HPLC-MS. Dots, independent samples from n=3 experiments. Errors are SEM.

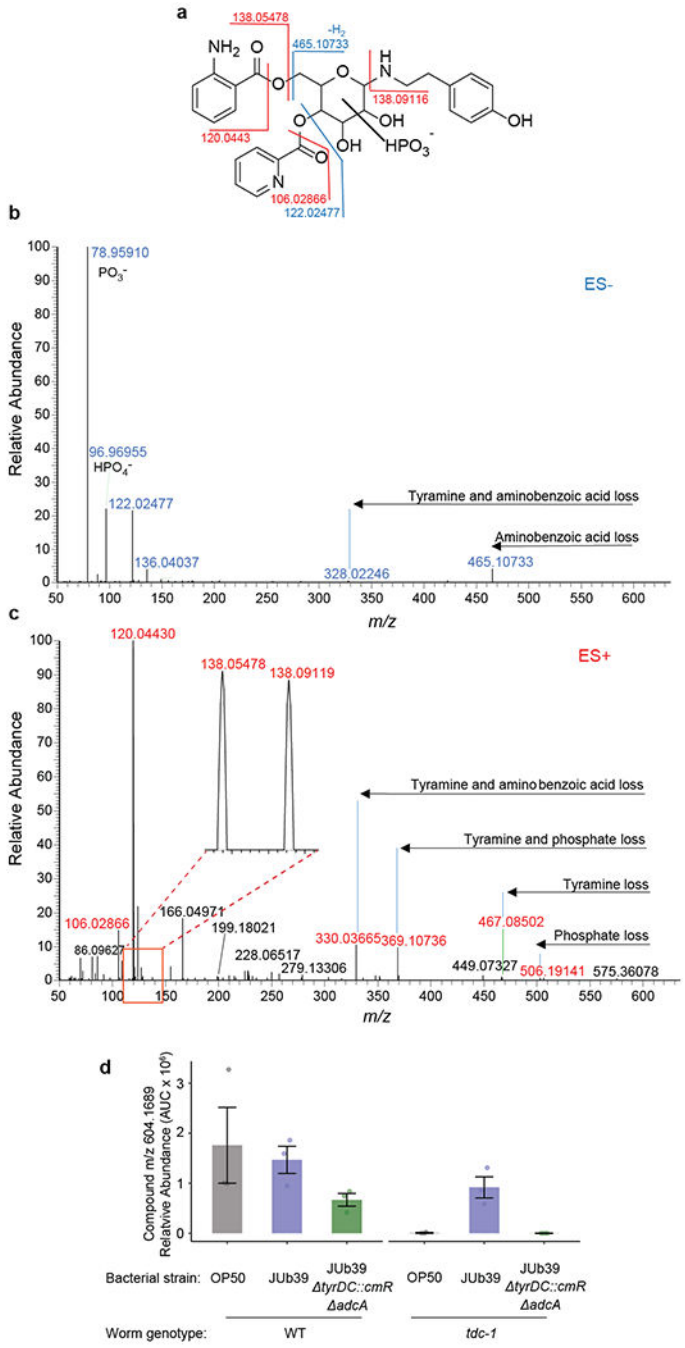

Extended Data Fig. 5. MS2 analysis and quantitation of TA-containing metabolite *m/z* 604.1689.

a, Major fragmentation reactions of *m/z* 604.1689 and resulting fragment ions. Stereochemistry and exact substitution pattern are unknown. The shown structure is based on fragmentation and stable isotope incorporation. **b-c,** MS2 spectra obtained in **(b)** negative- and **(c)** positive-ion mode. Representative data are shown from at least three biologically independent experiments. **d,** Quantification of *m/z* 604.1689 in wild-type and *tdc-1* worms fed the indicated bacterial strains as determined by positive-ion ESI HPLC-MS. Dots, independent samples from n=3 experiments. Errors are SEM.

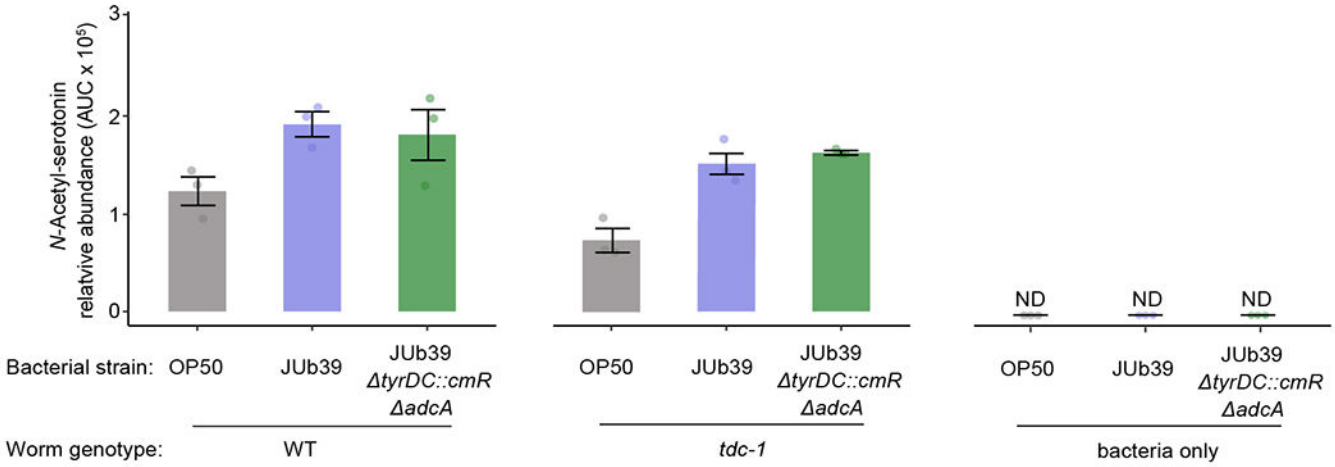

Extended Data Fig. 6.

Quantification of *N*-acetyl serotonin in worms fed the indicated bacteria, or in bacterial cultures alone, as determined by ESI+ HPLC-MS. Dots, independent samples from n=3 experiments. Errors are SEM.

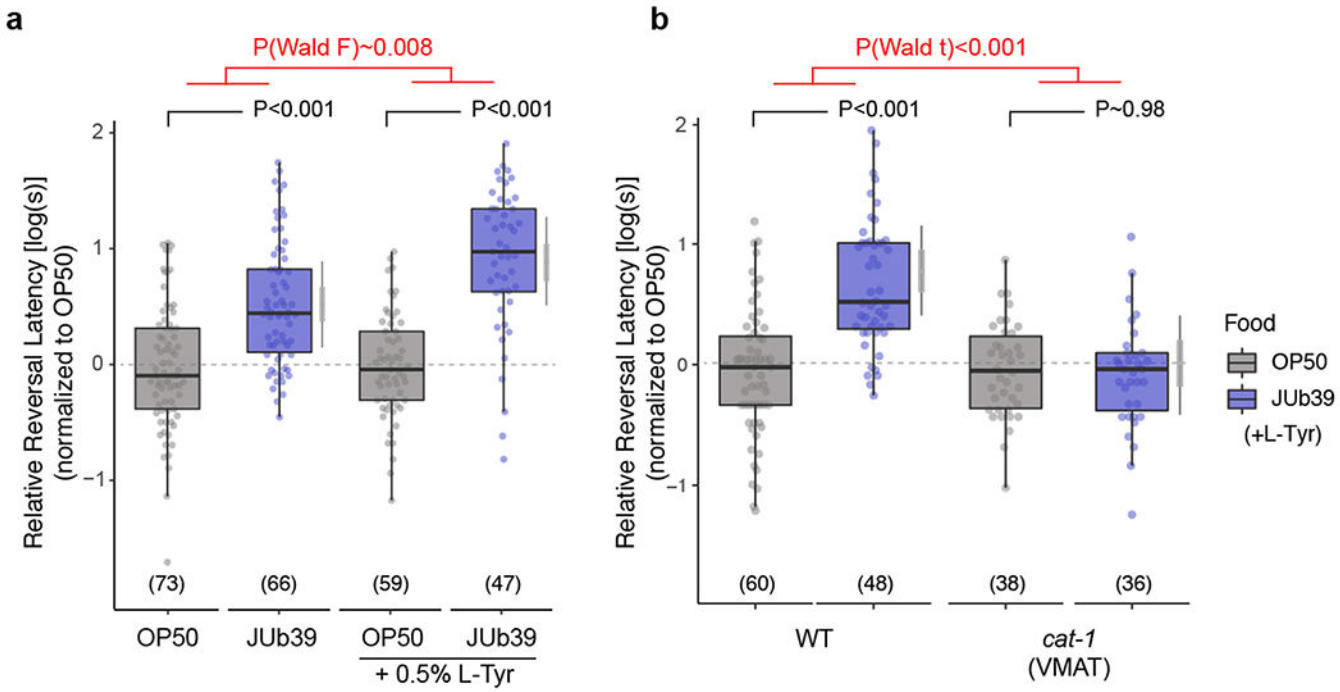

Extended Data Fig. 7. L-Tyr supplementation enhances octanol modulation.

a-b, Reversal response times of animals of the indicated genotypes grown on the indicated bacteria in control conditions **(a)** or supplemented with 0.5% L-Tyr **(a,b)** to 100% octanol using SOS assays. Dots, response time of single worms. Y-axis is $\log_{10}$-scaled for these log-normal distributed data, and normalized to the indicated control group for each experimental day. Numbers in parentheses, number of worms tested in assays over at least 3 independent days. Boxplot, median and quartiles, whiskers, data range (excluding outliers). Gray thin and thick vertical bars, Bayesian 95% and 66% credible intervals for the difference of means, respectively. *P*-values indicating comparisons of means relative to the OP50 control for each conditions are from a LMM with Tukey-type multivariate-t adjustment. *P*-value in red indicates Wald F-statistic (**a**) or Wald t-statistic (**b**) for the effect of L-Tyr supplementation (**a**) or genotype (**b**) on the magnitude of the JUb39 effect. Wild-type data in **(b)** are also shown in Fig. 2g.

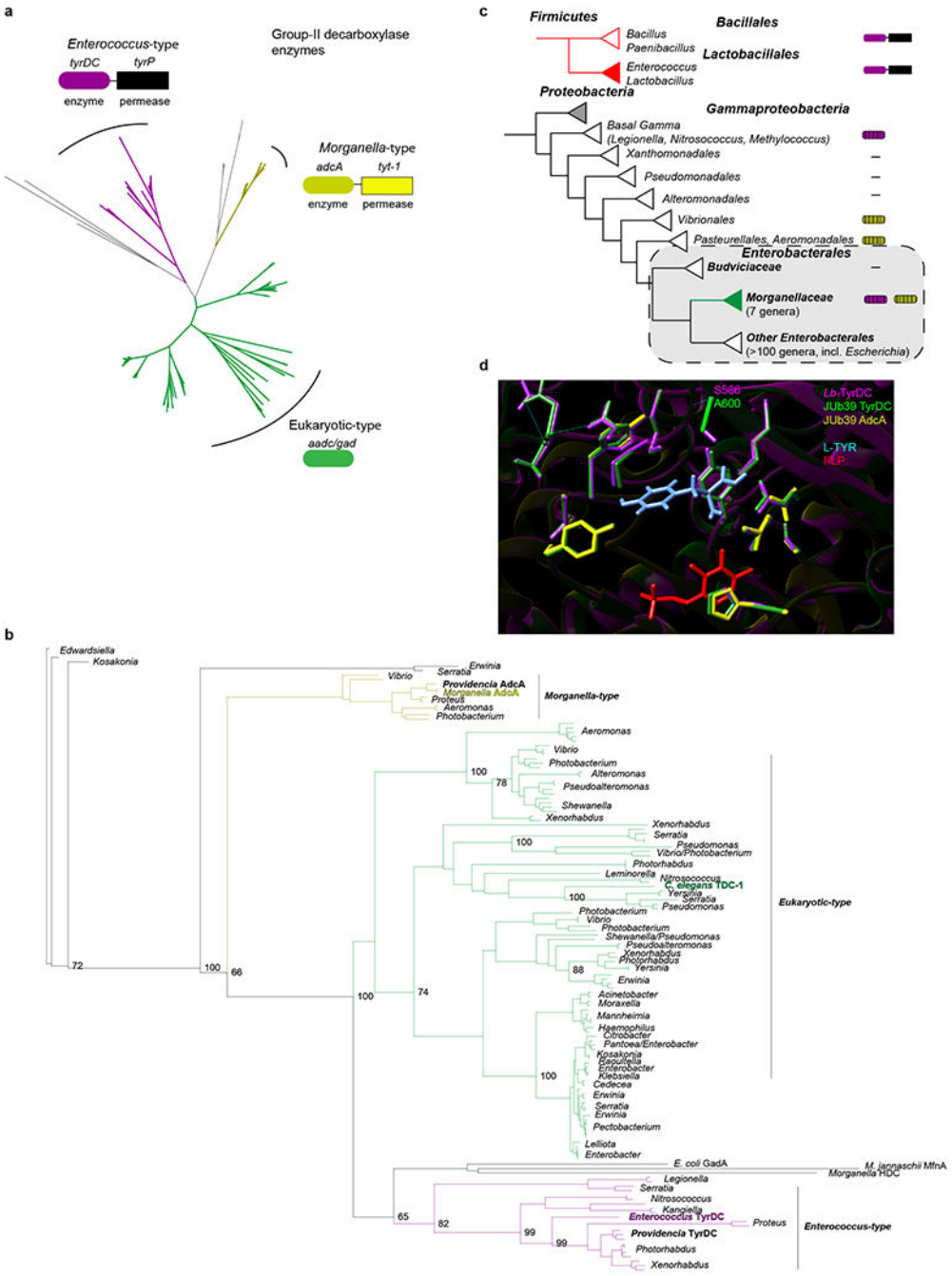

Extended Data Fig. 8. Phylogenetic analysis of group II decarboxylase genes in *Gammaproteobacteria*.

a, Neighbor-joining unrooted tree based on sequences identified via a BLAST search using *Enterococcus faecalis* TyrDC and *C. elegans* TDC-1. Initial tree indicates 3 major groups. Representative enzymes and operon structures for each group are indicated by colored boxes. **b,** Bootstrapped maximum likelihood phylogeny using PhyML and Phylomizer pipeline. Maximum of two highly similar sequences per genus were included after each BLAST search. Genera are indicated to the right. Numbers on branch-points matching this

tree out of 100 bootstrap replicates are indicated at values >60. Group representatives from **(a)** are indicated in corresponding colors. *Providencia* and *C. elegans* sequences discussed in this work are indicated in bold. Accession numbers and BLAST metrics are listed in SI Table 1. **c,** Presence of *tyrDC* and *adcA* among complete genomes in *Gammaproteobacteria*. Linked boxes indicate organization in an operon. Hatched shading indicates variable presence among genera. Colored triangles indicate taxa of interest. **d,** Homology-based model of the TyrDC catalytic domain in *Providencia* based on the *Lb*-TyrDC crystal structure[36] using SWISS-MODEL (https://swissmodel.expasy.org). Residues in magenta, green and yellow are from *Lb*-TyrDC, JUb39-TyrDC, and JUb39-AdcA, respectively. PLP is depicted in red and L-Tyr (manually docked for illustration) is indicated in light blue. Position of A600/S586[36] in JUb39 TyrDC and *Lb*-TyrDC are indicated.

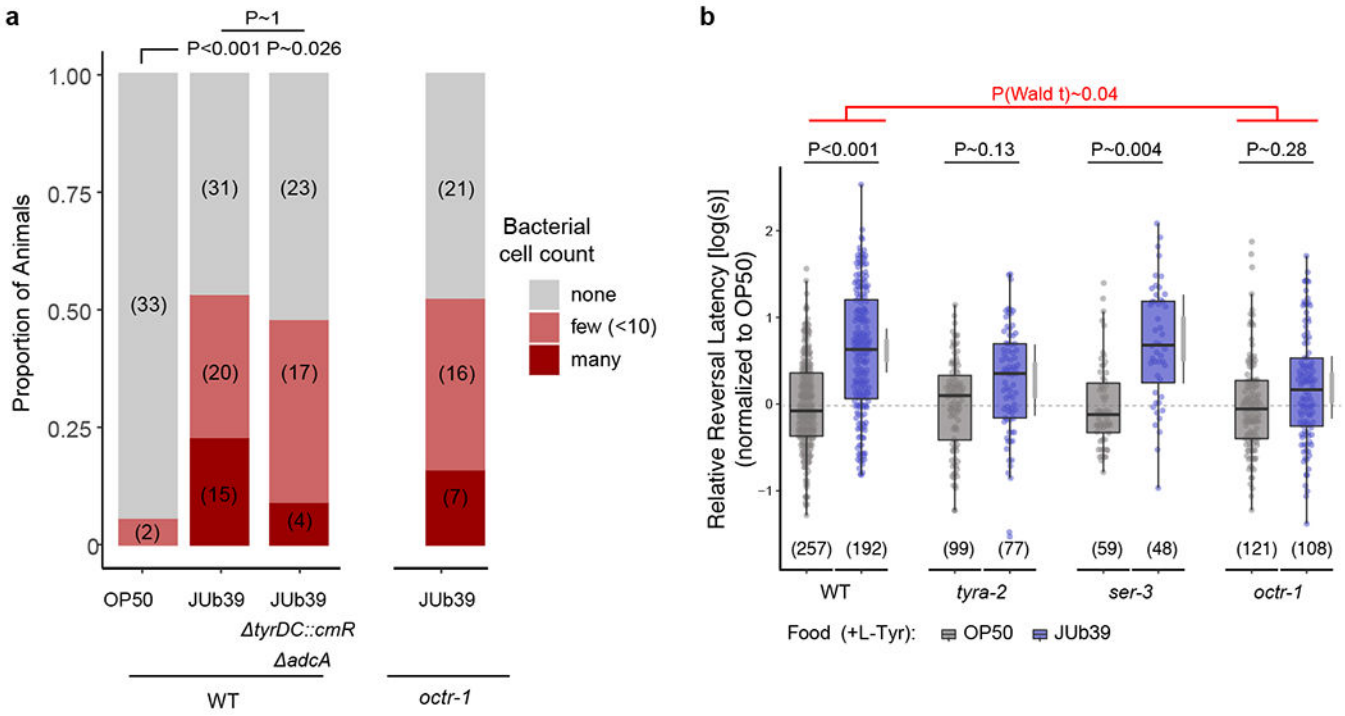

Extended Data Fig. 9. Disruption of JUb39 TA production or host OA receptor signaling affects octanol modulation without altering intestinal bacterial cell numbers.

a, Presence of mCherry-expressing bacteria in the posterior intestines of young adult wild-type or *octr-1* mutant animals. Bars show proportion of animals with the indicated distribution of bacterial cells present in animals grown on shown bacteria. Numbers in parentheses, number of animals. *P*-value is derived from an ordinal regression. **b,** Reversal response latency of animals of the indicated genotypes grown on the shown bacteria in control conditions of NGM + 0.5% L-Tyr to 100% octanol using SOS assays. Dots, response time of single worms. Y-axis is $\log_{10}$-scaled for these log-normal distributed data, and normalized to the indicated control group for each experimental day. Numbers in parentheses, number of worms tested in assays over at least 3 independent days. Boxplot, median and quartiles, whiskers, data range (excluding outliers). Gray thin and thick vertical bars, Bayesian 95% and 66% credible intervals for the difference of means, respectively. *P*-

values between indicated conditions are from a LMM with Tukey-type multivariate-t adjustment. *P*-values in red indicate Wald t-statistic representing the genotype x food interaction effect relative to WT.

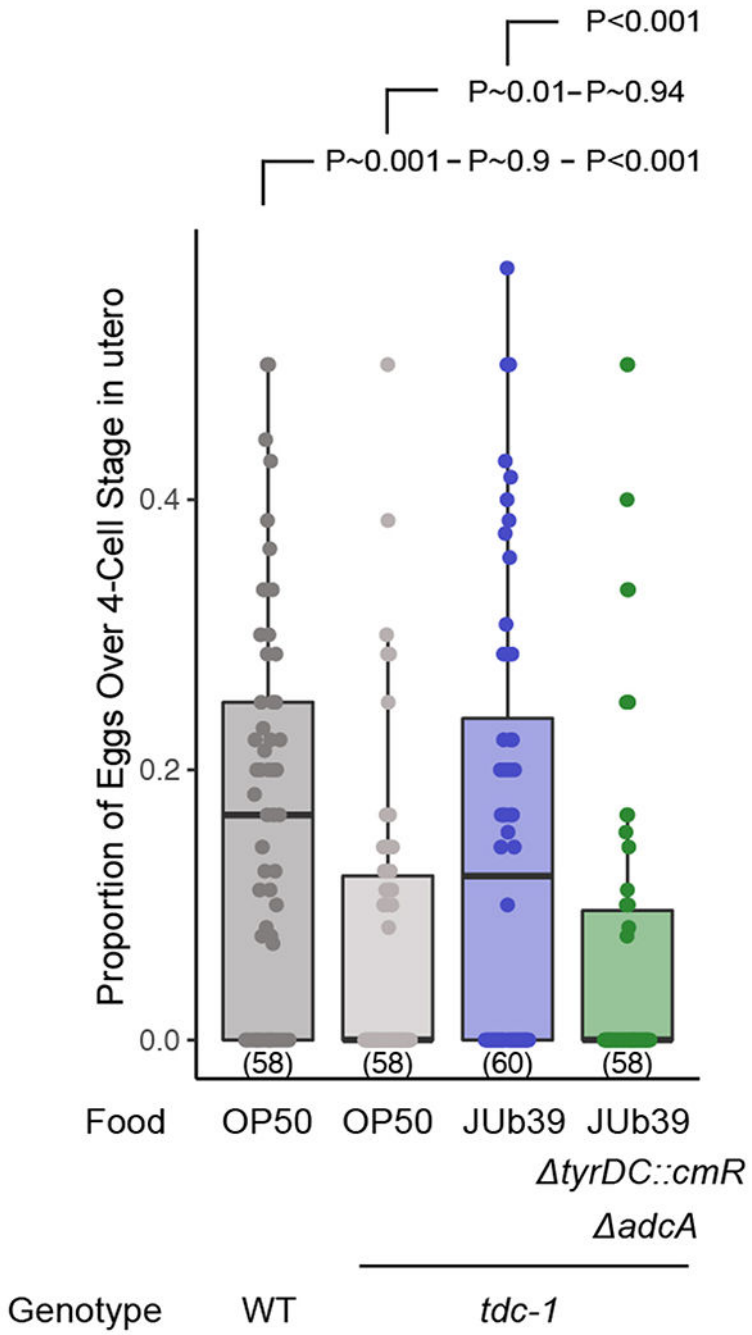

Extended Data Fig. 10. *Providencia*-derived TA complements the egg-laying defects of *C. elegans tdc-1* mutants.

Quantification of the age of eggs *in utero* of animals of the indicated genotypes grown on the shown bacterial strains. Dots, proportion of eggs at or older than the 4-cell stage in individual animals. Numbers in parentheses, total number of animals scored in three

independent experiments. Boxplot, median and quartiles, whiskers, data range (excluding outliers). *P*-values between the indicated conditions are from a binomial generalized linear mixed effects regression using a logit link function, with a post-hoc Tukey correction for multiple comparisons.

Supplementary Material

Refer to Web version on PubMed Central for supplementary material.

Acknowledgements

We thank Richard Komuniecki for the *octr-1* cDNA, Mark Alkema for the *tbh-1* promoter, multiple members of the *C. elegans* community for bacterial strains (listed in SI Table 2), and the *Caenorhabditis* Genetics Center for *C. elegans* strains. We are grateful to the Broad Institute for bacterial genome sequencing. We thank Max Helf for assistance with the Metaboseek software and Jingfang Yu and Henry Le for synthesis of *N*-succinyl neurotransmitter standards. We thank Sue Lovett, Laura Laranjo, Mark Alkema and the Sengupta lab for advice. We acknowledge the Sengupta lab, Cori Bargmann and Oliver Hobert for comments on the manuscript. This work was partly supported by the NIH (T32 NS007292 and F32 DC013711 – M.P.O., R01 GM088290 and R35 GM131877 – F.C.S., and R35 GM122463 and R21 NS101702 – P.S.), and the NSF (IOS 1655118 – P.S.).

References

1. Douglas AE Fundamentals of Microbiome Science: How Microbes Shape Animal Biology. (Princeton University Press, 2018).
2. Guo R, Chen L-H, Xing C & Liu T Pain regulation by gut microbiota: molecular mechanisms and therapeutic potential. Br. J. Anaesth 123, 637–654 (2019). [PubMed: 31551115]
3. Strandwitz P Neurotransmitter modulation by the gut microbiota. Brain Res. 1693, 128–133 (2018). [PubMed: 29903615]
4. Zhang J, Holdorf AD & Walhout AJ *C. elegans* and its bacterial diet as a model for systems-level understanding of host-microbiota interactions. Curr. Opin. Biotechnol 46, 74–80 (2017). [PubMed: 28189107]
5. Schulenburg H & Félix M-A The natural biotic environment of *Caenorhabditis elegans*. Genetics 206, 55–86 (2017). [PubMed: 28476862]
6. Meisel JD & Kim DH Behavioral avoidance of pathogenic bacteria by *Caenorhabditis elegans*. Trends Immunol. 35, 465–470 (2014). [PubMed: 25240986]
7. Samuel BS, Rowedder H, Braendle C, Félix M-A & Ruvkun G *Caenorhabditis elegans* responses to bacteria from its natural habitats. Proc. Natl. Acad. Sci. USA 113, E3941–9 (2016). [PubMed: 27317746]
8. Bargmann CI, Hartwieg E & Horvitz HR Odorant-selective genes and neurons mediate olfaction in *C. elegans*. Cell. 74, 515–527 (1993). [PubMed: 8348618]
9. Song B-M, Faumont S, Lockery S & Avery L Recognition of familiar food activates feeding via an endocrine serotonin signal in *Caenorhabditis elegans*. Elife 2, e00329 (2013). [PubMed: 23390589]
10. Chao MY, Komatsu H, Fukuto HS, Dionne HM & Hart AC Feeding status and serotonin rapidly and reversibly modulate a *Caenorhabditis elegans* chemosensory circuit. Proc. Natl. Acad. Sci. USA 101, 15512–15517 (2004). [PubMed: 15492222]
11. Liang B, Moussaif M, Kuan C-J, Gargus JJ & Sze JY Serotonin targets the DAF-16/FOXO signaling pathway to modulate stress responses. Cell Metab. 4, 429–440 (2006). [PubMed: 17141627]
12. Entchev EV et al. A gene-expression-based neural code for food abundance that modulates lifespan. Elife 4, e06259 (2015). [PubMed: 25962853]
13. Avery L & Shtonda BB Food transport in the *C. elegans* pharynx. J. Exp. Biol 206, 2441–2457 (2003). [PubMed: 12796460]
14. Avery L The genetics of feeding in *Caenorhabditis elegans*. Genetics 133, 897–917 (1993). [PubMed: 8462849]

15. Berg M et al. Assembly of the *Caenorhabditis elegans* gut microbiota from diverse soil microbial environments. ISME J. 10, 1998–2009 (2016). [PubMed: 26800234]
16. Dirksen P et al. The native microbiome of the nematode Caenorhabditis elegans: gateway to a new host-microbiome model. BMC Biol. 14, 38 (2016). [PubMed: 27160191]
17. Tan M-W, Mahajan-Miklos S & Ausubel FM Killing of *Caenorhabditis elegans* by *Pseudomonas aeruginosa* used to model mammalian bacterial pathogenesis. Proc. Natl. Acad. Sci. USA 96, 715–720 (1999). [PubMed: 9892699]
18. Irazoqui JE et al. Distinct pathogenesis and host responses during infection of C. elegans by P. aeruginosa and S. aureus. PLoS Pathog. 6, e1000982 (2010). [PubMed: 20617181]
19. Wragg RT et al. Tyramine and octopamine independently inhibit serotonin-stimulated aversive behaviors in *Caenorhabditis elegans* through two novel amine receptors. J. Neurosci. 27, 13402–13412 (2007). [PubMed: 18057198]
20. Mills H et al. Monoamines and neuropeptides interact to inhibit aversive behaviour in *Caenorhabditis elegans*. EMBO J. 31, 667–678 (2012). [PubMed: 22124329]
21. Harris GP et al. The monoaminergic modulation of sensory-mediated aversive responses in *Caenorhabditis elegans* requires glutamatergic/peptidergic cotransmission. J. Neurosci. 30, 7889–7899 (2010). [PubMed: 20534837]
22. Ezak MJ & Ferkey DM The C. elegans D2-Like dopamine receptor DOP-3 decreases behavioral sensitivity to the olfactory stimulus 1-octanol. PLoS ONE 5, e9487 (2010). [PubMed: 20209143]
23. Ezcurra M, Tanizawa Y, Swoboda P & Schafer WR Food sensitizes *C. elegans* avoidance behaviours through acute dopamine signalling. EMBO J. 30, 1110–1122 (2011). [PubMed: 21304491]
24. Alkema MJ, Hunter-Ensor M, Ringstad N & Horvitz HR Tyramine functions independently of octopamine in the *Caenorhabditis elegans* nervous system. Neuron 46, 247–260 (2005). [PubMed: 15848803]
25. Lints R & Emmons SW Patterning of dopaminergic neurotransmitter identity among *Caenorhabditis elegans* ray sensory neurons by a TGFbeta family signaling pathway and a Hox gene. Development 126, 5819–5831 (1999). [PubMed: 10572056]
26. Sze JY, Victor M, Loer C, Shi Y & Ruvkun G Food and metabolic signalling defects in a *Caenorhabditis elegans* serotonin-synthesis mutant. Nature 403, 560–564 (2000). [PubMed: 10676966]
27. Troemel ER, Chou JH, Dwyer ND, Colbert HA & Bargmann CI Divergent seven transmembrane receptors are candidate chemosensory receptors in *C. elegans*. Cell 83, 207–218 (1995). [PubMed: 7585938]
28. Artyukhin AB et al. Succinylated octopamine ascarosides and a new pathway of biogenic amine metabolism in *Caenorhabditis elegans*. J. Biol. Chem 288, 18778–18783 (2013). [PubMed: 23689506]
29. Pugin B et al. A wide diversity of bacteria from the human gut produces and degrades biogenic amines. Microb. Ecol. Health Dis 28, 1353881 (2017). [PubMed: 28959180]
30. Barbieri F, Montanari C, Gardini F & Tabanelli G Biogenic amine production by lactic acid bacteria: a review. Food 8, 17 (2019).
31. Marcobal Á, Martín-Álvarez PJ, Moreno-Arribas MV & Muñoz R A multifactorial design for studying factors influencing growth and tyramine production of the lactic acid bacteria *Lactobacillus brevis* CECT 4669 and *Enterococcus faecium* BIFI-58. Res. Microbiol 157, 417–424 (2006). [PubMed: 16488576]
32. Duerr JS et al. The *cat-1* gene of *Caenorhabditis elegans* encodes a vesicular monoamine transporter required for specific monoamine-dependent behaviors. J. Neurosci 19, 72–84 (1999). [PubMed: 9870940]
33. Sandmeier E, Hale TI & Christen P Multiple evolutionary origin of pyridoxal-5'-phosphate-dependent amino acid decarboxylases. Eur. J. Biochem 221, 997–1002 (1994). [PubMed: 8181483]
34. Connil N et al. Identification of the Enterococcus faecalis Tyrosine decarboxylase operon involved in tyramine production. Appl. Environ. Microb 68, 3537–3544 (2002).

35. Linares DM, Fernández M, Martín MC & Alvarez MA Tyramine biosynthesis in Enterococcus durans is transcriptionally regulated by the extracellular pH and tyrosine concentration. Microb. Biotechnol 2, 625–633 (2009). [PubMed: 21255297]
36. Zhu H et al. Crystal structure of tyrosine decarboxylase and identification of key residues involved in conformational swing and substrate binding. Sci. Rep 6, 27779 (2016). [PubMed: 27292129]
37. Quick M, et al. State-dependent conformations of the translocation pathway in the tyrosine transporter Tyt1, a novel neurotransmitter:sodium symporter from *Fusobacterium nucleatum*. J. Biol. Chem 281, 26444–26454 (2006). [PubMed: 16798738]
38. Collins KM et al. Activity of the C. elegans egg-laying behavior circuit is controlled by competing activation and feedback inhibition. Elife 5, e21126 (2016). [PubMed: 27849154]
39. Rex E et al. TYRA-2 (F01E11.5): A Caenorhabditis elegans tyramine receptor expressed in the MC and NSM pharyngeal neurons. J. Neurochem 94, 181–191 (2005). [PubMed: 15953361]
40. Sun J, Singh V, Kajino-Sakamoto R & Aballay A Neuronal GPCR controls innate immunity by regulating noncanonical unfolded protein response genes. Science 332, 729–732 (2011). [PubMed: 21474712]
41. Elgaali H et al. Comparison of long-chain alcohols and other volatile compounds emitted from food-borne and related Gram positive and Gram negative bacteria. J. Basic Microbiol 42, 373–380 (2002). [PubMed: 12442299]
42. Worthy SE et al. Identification of attractive odorants released by preferred bacterial food found in the natural habitats of C. elegans. PLoS ONE 13, e0201158 (2018). [PubMed: 30036396]
43. Yoshida K et al. Odour concentration-dependent olfactory preference change in *C. elegans*. Nat. Commun 3, 739 (2012). [PubMed: 22415830]
44. Zhang F et al. *Caenorhabditis elegans* as a model for microbiome research. Front. Microbiol 8, 485 (2017). [PubMed: 28386252]
45. Leitão-Gonçalves R et al. Commensal bacteria and essential amino acids control food choice behavior and reproduction. PLoS Biol. 15, e2000862 (2017). [PubMed: 28441450]
46. Pais IS, Valente RS, Sporniak M & Teixeira L *Drosophila melanogaster* establishes a species-specific mutualistic interaction with stable gut-colonizing bacteria. PLoS Biol. 16, e2005710 (2018). [PubMed: 29975680]
47. Henriques SF et al. Metabolic cross-feeding allows a gut microbial community to overcome detrimental diets and alter host behaviour. BioRxiv doi:10.1101/821892 (2019).
48. Breton J et al. Gut commensal *E. coli* proteins activate host satiety pathways following nutrient-induced bacterial growth. Cell Metab. 23, 324–334 (2016). [PubMed: 26621107]
49. Fetissov SO Role of the gut microbiota in host appetite control: bacterial growth to animal feeding behaviour. Nat. Rev. Endocrinol 13, 11–25 (2017). [PubMed: 27616451]

Methods References

50. Blomfield IC, Vaughn V, Rest RF & Eisenstein BI Allelic exchange in *Escherichia coli* using the *Bacillus subtilis sacB* gene and a temperature-sensitive pSC101 replicon. Mol. Microbiol 5, 1447–1457 (1991). [PubMed: 1686293]
51. Jiang Y et al. Multigene editing in the Escherichia coli genome via the CRISPR-Cas9 system. Appl. Environ. Microb 81, 2506–2514 (2015).
52. Marx CJ Development of a broad-host-range sacB-based vector for unmarked allelic exchange. BMC Res. Notes 1, 1 (2008). [PubMed: 18710539]
53. Barbier M & Damron FH Rainbow Vectors for broad-range bacterial fluorescence labeling. PLoS ONE 11, e0146827 (2016). [PubMed: 26937640]
54. Alegado RA & Tan M-W Resistance to antimicrobial peptides contributes to persistence of *Salmonella typhimurium* in the *C. elegans* intestine. Cell Microbiol. 10, 1259–1273 (2008). [PubMed: 18221392]
55. Troemel ER, Kimmel BE & Bargmann CI Reprogramming chemotaxis responses: sensory neurons define olfactory preferences in *C. elegans*. Cell 91, 161–169 (1997). [PubMed: 9346234]

56. Koren S, Walenz BP, Berlin K, Miller JR & Phillippy AM Canu: scalable and accurate long-read assembly via adaptive k-mer weighting and repeat separation. Genome Res. 27, 722–736 (2017). [PubMed: 28298431]
57. Hunt M et al. Circlator: automated circularization of genome assemblies using long sequencing reads. Genome Biol. 16, 294 (2015). [PubMed: 26714481]
58. Edgar RC MUSCLE: multiple sequence alignment with high accuracy and high throughput. Nucleic Acids Res. 35, 1792–1797 (2004).
59. Katoh K, Misawa K, Kuma K & Miyata T MAFFT: a novel method for rapid multiple sequence alignment based on fast Fourier transform. Nucleic Acids Res. 30, 3059–3066 (2002). [PubMed: 12136088]
60. Lassmann T & Sonnhammer ELL, Kalign – an accurate and fast multiple sequence alignment algorithm. BMC Bioinformatics 6, 298 (2005). [PubMed: 16343337]
61. Capella-Gutierrez S, Silla-Martinez JM & Gabaldon T Bioinformatics 25, 1972–1973 (2009). [PubMed: 19505945]
62. Guindon S et al. New algorithms and methods to estimate maximum-likelihood phylogenies: assessing the performance of PhyML 3.0. Syst. Biol 59, 307–321 (2010). [PubMed: 20525638]
63. Darriba D, Taboada GL, Doallo R & Posada D ProtTest 3: fast selection of best-fit models of protein evolution. Bioinformatics 27, 1164–1165 (2011). [PubMed: 21335321]
64. Waterhouse A et al. SWISS-MODEL: homology modelling of protein structures and complexes. Nucleic Acids Res. 46, W296–W303 (2018). [PubMed: 29788355]
65. Petersen EF et al. UCSF Chimera—a visualization system for exploratory research and analysis. J. Comput. Chem 25, 1605–1612 (2004). [PubMed: 15264254]
66. R Core Team. R: A language and environment for statistical computing. R Foundation for Statistical Computing, Vienna, Austria.
67. RStudio Team. RStudio: integrated development for R. RStudio Inc., Boston, MA.
68. Bates D, Maechler M, Bolker B & Walker S Fitting linear mixed-effects models using lme4. J. Stat. Softw 67, 1–48 (2015).
69. Lenth R, emmeans: estimated marginal means, aka least-squares means. R package version 1.4.5. (2020) https://CRAN.R-project.org/package=emmeans
70. Halekoh U & Højsgaard S A Kenward-Roger approximation and parametric bootstrap methods for tests in linear mixed models - the R package pbkrtest. J. Stat. Softw 59, 1–30 (2014). [PubMed: 26917999]
71. Kuznetsova A, Brockhoff PB & Christensen RHB lmerTest package: tests in linear mixed effects models. J. Stat Softw 82, 1–26 (2017).
72. Fox J & Weisberg S An R Companion to Applied Regression, Third Edition (Sage Press, 2019).
73. Goodrich B, Gabry J, Ali I & Brilleman S rstanarm: Bayesian applied regression modeling via Stan. (2020).
74. Plummer M, Best N, Cowles K & Vines K CODA: convergence diagnosis and output analysis for MCMC. R News 6, 7–11 (2006).
75. Gabry J, Simpson D, Vehtari A, Betancourt M & Gelman A Visualization in Bayesian workflow. J. R. Stat. Soc. A 182, 389–402 (2019).
76. Kay M tidybayes: tidy data and geoms for Bayesian models. (2020). doi: 10.5281/zenodo.1308151 (URL: 10.5281/zenodo.1308151).
77. Venables WN & Ripley BD Modern Applied Statistics with S. Fourth Edition (Springer, 2002) ISBN 0-387-95457-0.
78. Helf M Metaboseek: an interactive, browser-based tool to analyze your mass spectrometry data. (2019). doi: 10.5281/zenodo.3360087 (URL: 10.5281/zenodo.3360087).
79. Smith CA, Want EJ, O'Maille G, Abagyan R & Siuzdak G XCMS: processing mass spectrometry data for metabolite profiling using nonlinear peak alignment, matching, and identification. Anal. Chem 78, 779–787 (2006). [PubMed: 16448051]

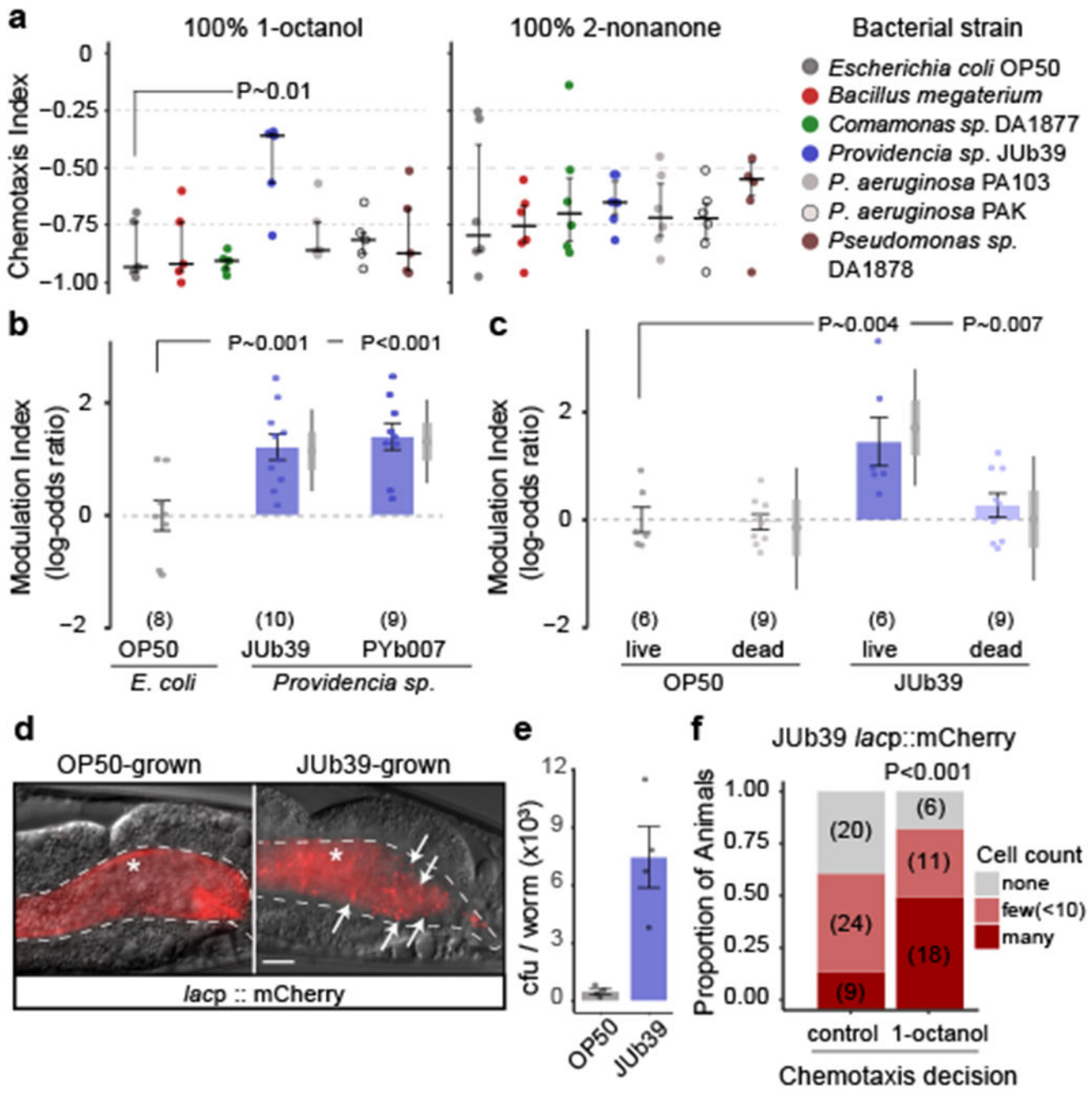

Fig. 1. *Providencia* colonizes the *C. elegans* intestine and modulates octanol avoidance.

a, Long-range chemotaxis assays (Extended Data Fig. 1a) of *C. elegans* grown on the indicated bacterial strains to aversive odors. Chemotaxis index (CI) = (animals at odorant – animals at control)/total animals. Dots, CI from single assays of approximately 100 animals. Horizontal line, median; errors, 1st and 3rd quartiles. *P*-value is derived from *z*-statistic from a binomial general linearized mixed-effects model (GLMM) with random intercepts for assay plate and date and with false discovery rate (FDR) for post-hoc comparisons (two-sided test). n = 5 and 6 independent experiments for octanol and nonanone assays, respectively, over 3 days. **b-c**, Modulation index of worms in response to 100% octanol.

'Dead' **(c),** bacteria pre-treated with gentamicin. Modulation index, the log odds-ratio of the proportion of worms at octanol vs control of each condition normalized to the OP50-grown condition per independent day (gray dashed line). Positive numbers, reduced octanol avoidance. Errors are SEM. Gray vertical bars, Bayesian 95% and 66% credible intervals, respectively. *P*-values, two-sided GLMM with Dunnett-type **(b)**, and Tukey-type multivariate-t adjustment **(c)**. Numbers in parentheses, independent experiments over 3-5 days with approximately 100 animals each (also see Extended Data Fig. 9a). **d,** mCherry-expressing bacteria in the posterior intestines of young adults. Arrows, intact cells, asterisk, diffuse intestinal fluorescence, dashed lines, intestinal boundary. Anterior at left. Scale bar, 10 μm. **e,** Intestinal bacterial load in animals grown on the indicated bacterial strains. Dots, estimation of bacterial load in colony forming units (cfu) of 10 worms; n = 4 independent samples (see Methods). Data are mean ± SEM. **f,** Proportion of animals that migrated to 100% octanol or control in chemotaxis assays with indicated distribution of mCherry-expressing JUb39 cells. Numbers in parentheses, number of animals; 3 independent assays. *P*-value is derived from an ordinal regression *z*-statistic, using number of animals.

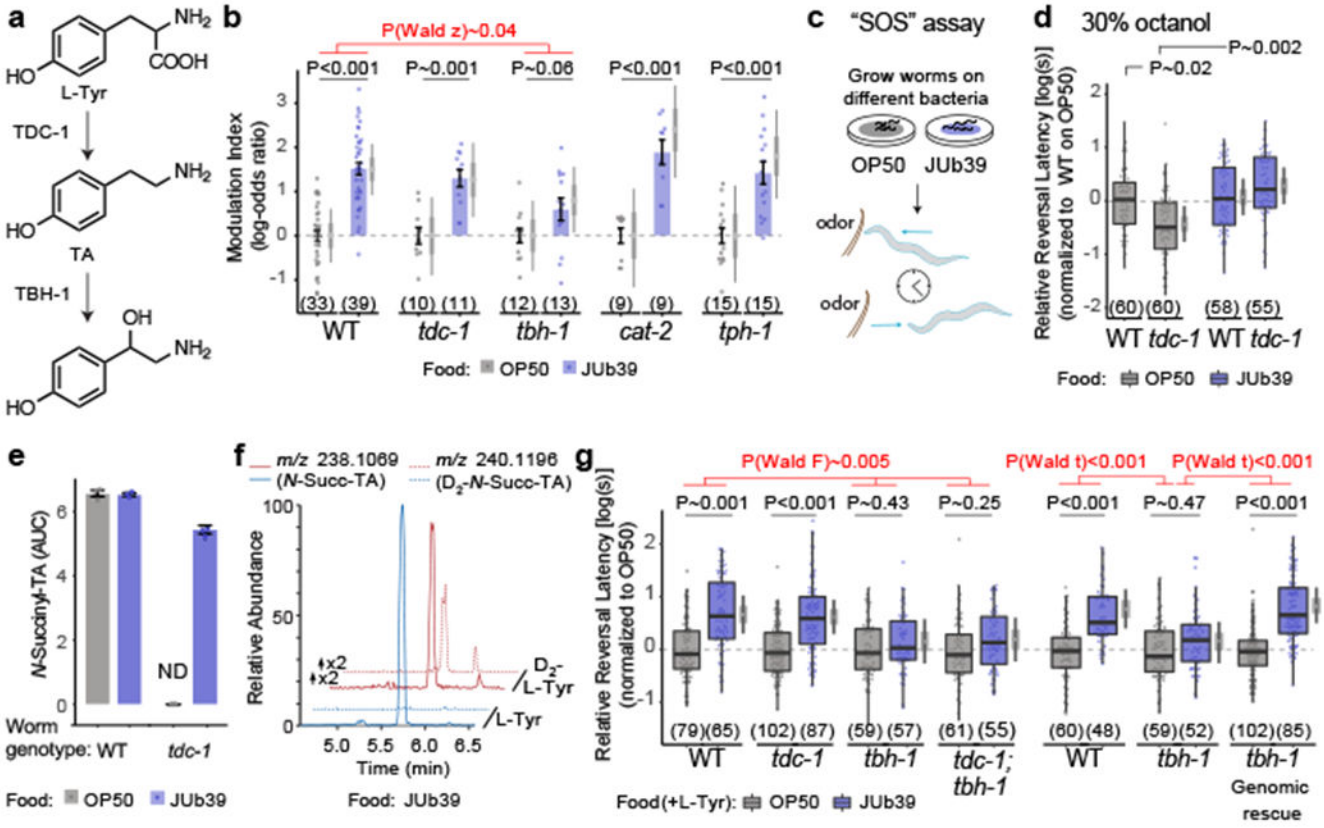

Fig. 2. *Providencia*-produced TA compensates for loss of *C. elegans tdc-1*.

a, Biosynthesis of TA and OA in *C. elegans*[24]. **b**, Modulation index of animals in response to 100% octanol. Dots, individual chemotaxis assays with approximately 100 animals each. Numbers in parentheses, number of independent assays over at least 3 independent days. Y-axis is log-odds (logit) scale, normalized to OP50 for each day (gray dashed lines). Errors are SEM. Gray thin and thick vertical bars, Bayesian 95% and 66% credible intervals, respectively. *P*-values, GLMM with Dunnett-type multivariate-t adjustment. *P*-value in red, Wald *z*-statistic for the magnitude of the JUb39 effect in *tbh-1* compared to wild-type. **c,** Cartoon of SOS assay [10,27]. **d, g,** Reversal response latency of animals on NGM without (**d**) or with 0.5% L-Tyr (**g**) in response to 30% (**d**) or 100% octanol (**g**) in SOS assays. Dots, response time of single animals. Y-axis is $\log_{10}$-scaled, normalized to the indicated control group for each experimental day. Numbers in parentheses, number of worms tested in assays over at least 3 independent days. Boxplot, median and quartiles, whiskers, data range (excluding outliers). Gray vertical bars, Bayesian 95% and 66% credible intervals for the difference of means, respectively. *P*-values, linear-mixed effects regression on log-transformed data (LMM). *P*-values in red (**g**), Wald F-statistic (left) or Wald t-statistic (right) for the effect of the indicated genotypes on the magnitude of the JUb39 effect. Data from wild type in (**g,** right) are repeated in Extended Data Fig. 7b. Alleles: *tbh-1(ok1196)* (**g,** left), *tbh-1(n3247)* (**g,** right). **e,** Quantification of *N*-succinyl TA. Dots, area under the curve (AUC) from three biologically independent experiments. Data are mean ± SEM. ND, not detected. **f,** HPLC-MS (ESI+) ion chromatograms for *N*-succinyl TA or D_2-*N*-succinyl TA in worms grown on JUb39 with the indicated amino-acid supplementation. Chromatograms for

D_2-L-Tyr fed worms are scaled two-fold relative to L-Tyr feeding. Statistical comparisons are two-sided.

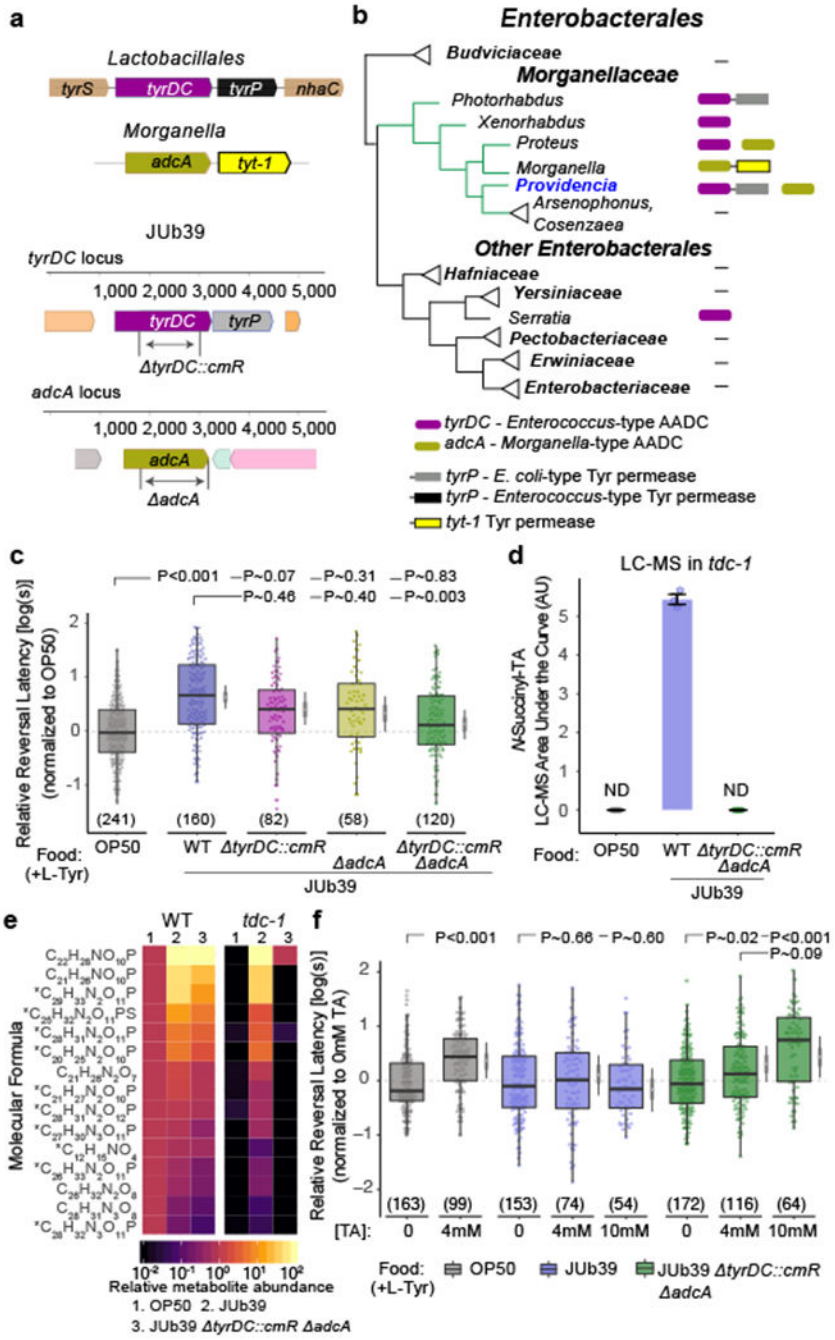

Fig. 3. Two *Providencia* AADC enzymes act redundantly to modulate octanol avoidance.

a, Cartoons depicting the *tyrDC* locus in *Lactobacillales,* the *adcA* locus in *Morganella* (top), and corresponding loci including engineered muations in JUb39 (bottom). **b,** Presence of *tyrDC, adcA, E.coli*-type *tyrP* and *Morganella*-type *tyt-1* at the family and genus level among *Enterobacterales*. Linked boxes indicate organization in an operon. **c, f,** Reversal response latency of wild-type *C. elegans* grown on the indicated bacterial genotypes in NGM + 0.5% L-Tyr (**c**) or supplemented with the indicated concentrations of TA **(f)** to 100% octanol using SOS assays. Dots, response time of single worms. Y-axis is $\log_{10}$-scaled

and normalized to the indicated control group for each experimental day (gray dashed line). Numbers in parentheses, number of worms tested in assays over at least 3 independent days. Boxplot, median and quartiles, whiskers, data range (excluding outliers). Gray thin and thick vertical bars at right, Bayesian 95% and 66% credible intervals for the difference of means, respectively. *P*-values between indicated conditions are from a LMM with Tukey-type multivariate-t adjustment. **d**, Quantification of *N*-succinyl TA in *tdc-1* mutant animals grown on the indicated bacterial strains. OP50 and JUb39 data are repeated from Fig. 2e. Dots, area under the curve (AUC) from each of 3 biologically independent experiments. Data are mean ± SEM. ND, not detected. **e,** Heatmap showing mean abundance of TA-derived compounds of indicated molecular formula detected in N2 wild-type and *tdc-1* mutant worms grown on the indicated bacterial strains, relative to N2 worms grown on OP50. Means are calculated from 3 independent experiments. Asterisks indicate D_2-containing compounds confirmed using D_2-L-tyrosine supplementation (Fig. 2f).

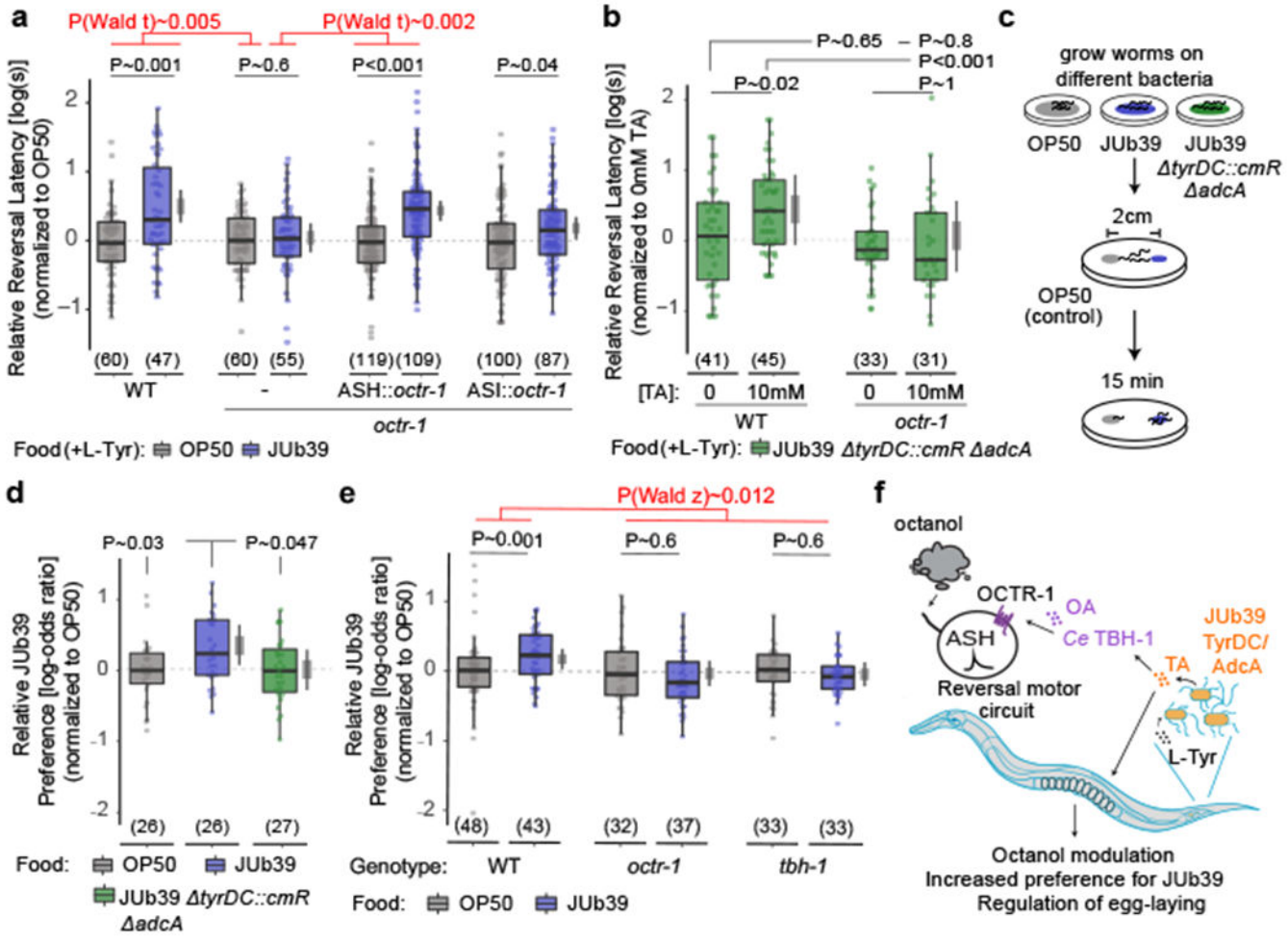

Fig. 4. Modulation of octanol avoidance by *Providencia* requires the OCTR-1 OA receptor in the ASH sensory neurons.

a-b, Reversal response latency of animals of the indicated worm genotypes grown on the indicated bacteria on NGM + 0.5% L-Tyr **(a)** and supplemented with the indicated concentrations of TA **(b)** to 100% octanol using SOS assays. Dots, response time of single worms. Y-axis is $\log_{10}$-scaled and normalized to the indicated control group **(a)** or to the wild-type control **(b)** for each experimental day. Numbers in parentheses, number of worms tested in assays over at least 3 independent days. Wild-type *octr-1* sequences were expressed in ASH and ASI under the *srv-11* and *srg-47* promoters, respectively. Boxplot, median and quartiles, whiskers, data range (excluding outliers). Gray thin and thick vertical bars, Bayesian 95% and 66% credible intervals for the difference of means. *P*-values between indicated conditions are from a LMM with Tukey-type multivariate-t adjustment. *P*-values in red, Wald t-statistic representing the genotype x food interaction effect relative to WT. **c,** Cartoon depicting short-range bacterial choice assay. **d-e,** Relative preference index of wild-type or mutant animals grown on the indicated bacteria for the test bacteria JUb39. Data are normalized to the OP50 control condition for each genotype. Dots, single assays of at least 10 animals. Numbers in parentheses, number of assays over at least 5 independent days. Y-axis is on log-odds ratio (logit) scale. Errors are SEM. Gray thin and thick vertical bars,

Bayesian 95% and 66% credible intervals, respectively. *P*-values represent difference of means relative to JUb39-grown animals from a GLMM with Dunnett-type multivariate-t adjustment. *P*-value in red, Wald z-statistic representing the genotype x food interaction effect relative to WT **(e)**. Allele used: *tbh-1(n3247)* **(e)**. **f,** Cartoon of working model.